



Ophicalcites from the northern Pyrenean belt: a field, petrographic and stable isotope study

Camille Clerc, Philippe Boulvais, Yves Lagabrielle, Michel de Saint Blanquat

► To cite this version:

Camille Clerc, Philippe Boulvais, Yves Lagabrielle, Michel de Saint Blanquat. Ophicalcites from the northern Pyrenean belt: a field, petrographic and stable isotope study. *International Journal of Earth Sciences*, 2014, 103 (21), pp.141-163. 10.1007/s00531-013-0927-z . insu-00944405

HAL Id: insu-00944405

<https://hal-insu.archives-ouvertes.fr/insu-00944405>

Submitted on 10 Feb 2014

HAL is a multi-disciplinary open access archive for the deposit and dissemination of scientific research documents, whether they are published or not. The documents may come from teaching and research institutions in France or abroad, or from public or private research centers.

L'archive ouverte pluridisciplinaire **HAL**, est destinée au dépôt et à la diffusion de documents scientifiques de niveau recherche, publiés ou non, émanant des établissements d'enseignement et de recherche français ou étrangers, des laboratoires publics ou privés.

Opicalcites from the Northern Pyrenean Belt: a field, petrographic and stable isotope study.

by:

Camille Clerc (1), Boulvais Philippe (2), Yves Lagabriele (3) and Michel de Saint Blanquat (4)

(1) Laboratoire de Géologie, CNRS-UMR 8538, Ecole Normale Supérieure, 24 rue Lhomond, 75231 Paris Cedex 5, France.

(2) Géosciences Rennes, CNRS-UMR 6118, Université de Rennes 1, Campus de Beaulieu, 35042, Rennes Cedex, France

(3) Géosciences Montpellier, CNRS-UMR 5243, Université de Montpellier 2, Place Eugène Bataillon, 34095 Montpellier, France

(4) GET, CNRS-UMR 5563, Université Paul Sabatier, 14 avenue Edouard Belin, 31400 Toulouse, France.

Corresponding author:

Camille Clerc

clerc@geologie.ens.fr

Abstract

Brecciated and fractured peridotites with a carbonate matrix, referred to as *ophicalcites*, are common features of mantle rocks exhumed in passive margins and mid-oceanic ridges. Ophicalcites have been found in close association with massive peridotites, which form the numerous ultramafic bodies scattered along the North Pyrenean Zone (NPZ), on the northern flank of the Pyrenean belt. We present the first field, textural and stable isotope characterization of these rocks. Our observations show that Pyrenean ophicalcites belong to three main types: (1) a wide variety of breccias composed of sorted or unsorted millimeter-to meter-sized clasts of fresh or oxidized ultramafic material, in a fine-grained calcitic matrix; (2) calcitic veins penetrating into fractured serpentine and fresh peridotite; and (3) pervasive substitution of serpentine minerals by calcite. Stable isotope analyses (O, C) have been conducted on the carbonate matrix, veins and clasts of samples from 12 Pyrenean ultramafic bodies. We show that the Pyrenean ophicalcites are the product of three distinct genetic processes: i) pervasive ophicalcite resulting from relatively deep and hot hydrothermal activity; ii) ophicalcites in veins resulting from tectonic fracturing and cooler hydrothermal activity; and iii) polymictic breccias resulting from sedimentary processes occurring after the exposure of subcontinental mantle as portions of the floor of basins which opened during the mid-Cretaceous. We highlight a major difference between the Eastern and Western Pyrenean ophicalcites belonging respectively to the sedimentary and to the hydrothermal types. Our data set points to a possible origin of the sedimentary ophicalcites in continental endorheic basins, but a post-depositional evolution by circulation of metamorphic fluids or an origin from relatively warm marine waters cannot be ruled out. Finally, we discuss the significance of such discrepancy in the characteristics of the NPZ ophicalcites in the frame of the variable exhumation history of the peridotites all along the Pyrenean realm.

49

50

51 **Key words:** ophicalcite, ophicarbonates, stable isotopes, oxygen, carbon, veins, matrices,
52 Pyrenees, Lherz, Urdach, mantle exhumation, tectonic fracturation, hydrothermalism,
53 sedimentary deposits.

I. Introduction

During uplift and exhumation of the sub-continental mantle, the peridotites are commonly serpentized through interactions with fluids, with direct consequences on their bulk density and their rheological, seismic, gravimetric and magnetic properties (Brun & Beslier 1996; Boschi et al. 2006). In oceanic and passive margin environments, besides serpentization, the peridotites show evidence of carbonation expressed through the occurrence of a bimodal, ultramafic and carbonate association known as ophicalcites or ophicarbonates (Spooner & Fyfe 1973; Bonatti et al. 1974; Dietrich et al. 1974; Gianelli & Principi 1977; Ohnenstetter 1979; Lemoine 1980; Cortesogno et al. 1981; Lagabriele & Cannat 1990). More recently, the carbonation of the exhumed mantle rocks has been clearly described as the last event affecting faulted rocks uprising along oceanic detachment faults at the axis of slow-spreading ridges (Picazo et al. 2012).

Ophicalcites were first discovered in the Ligurian Alps (Bonney 1879), and then described in many ophiolite sequences (see Artemyev & Zaykov 2010 and Bogoch 1987 for a comprehensive historical literature on ophicalcites). Ophicalcites commonly display large variations in the proportions of ultramafic and carbonate material. They range from in-situ fractured peridotites with carbonate infill, through clast-supported breccias with multiple generations of carbonate infilling and internal sediments, to matrix-supported breccias. Lemoine et al. (1987) distinguish two main types of ophicalcite. Ophicalcite type 1 (OC1) is represented by massive serpentinites exhibiting a dense mesh of calcite-infilled fractures. Ophicalcite type 2 (OC2) refers to sedimentary breccias having a calcitic matrix, often deposited above ophicalcite of type 1. The clasts comprise sorted or unsorted millimeter- to meter-sized fresh or oxidized ultramafic fragments. In some cases, exotic clasts of gabbroic or basaltic composition can be observed. The matrix of OC2 is either a fine-grained calcitic

sediment or a cement consisting of sparry calcite. It varies in color from red to pink and gray to green, depending on the chlorite or hematite content; sparry calcite is generally white. Opicalcites often record a polyphase history, revealed by different generations of cements and sediment infill, which can be highlighted by color changes, and bimodal grain distribution (Abbate et al. 1970; Bonatti et al. 1974; Bernoulli & Weissert 1985; Lemoine et al. 1987; Früh-Green et al. 1990).

Because of the wide variety of opicalcites and their occurrence in different oceanic or continental margin settings, it is important to recall that the term opicalcite does not refer to a genetic process, but to a generic rock-type. Among the processes invoked for their formation one group refers to endogenic evolution, involving various deep seated phenomena such as: (1) mantle originated gas seeps (Bonatti et al. 1974; Haggerty 1991; Kelemen et al. 2004); (2) magmatic intrusions (Cornelius 1912; Bailey & McCallien 1960); (3) contact and regional metamorphism (Peters 1965; Trommsdorff et al. 1980) and (4) hydrothermal fluid interactions (Cornelius 1912; Lavoie & Cousineau 1995; Artemyev & Zaykov 2010). Another group refers to surficial processes involving mechanical mixing of carbonates and ultramafic rocks through tectonic crushing, sedimentary reworking and gravity-driven infilling of veins and fractures (Bortolotti & Passerini 1970; Knipper 1978; Bernoulli & Weissert 1985; Früh-Green et al. 1990; Treves & Harper 1994; Treves et al. 1995; Knipper & Sharas'kin 1998).

In the French Pyrenees, opicalcites have been reported in some ultramafic bodies associated with mid-Cretaceous basins and recently re-interpreted as resulting from mantle exhumation during Mid-Cretaceous rifting (Lagabriele & Bodinier 2008; Lagabriele et al. 2010; Jammes et al. 2009; Clerc et al. 2012). In order to document and to characterize the variable typology of opicalcites and to decipher their origin with respect to exhumation processes, we have performed a comprehensive field, petrological and geochemical study of samples taken throughout the Pyrenees (fig. 1). We identify three types of opicalcites related to three

distinct genetic processes: i) pervasive ophicalcite resulting from replacement of ultramafic minerals due to relatively deep and hot hydrothermal activity, ii) ophicalcites as veins resulting from tectonic fracturing and cooler hydrothermal activity and iii) polymictic breccias resulting from syn-sedimentary processes. The first two types record the activity associated with the final emplacement of the peridotites, whereas the last one is associated with the final exhumation of mantle rocks as portions of the basement of newly formed basins.

II. Geological setting of the ultramafic Pyrenean bodies:

The Pyrenees are a narrow, 400 km long continental fold and thrust belt resulting from the collision of the northern edge of the Iberian Plate and the southern edge of the European Plate during the late Cretaceous to Tertiary (Choukroune & ECORS Team 1989; Muñoz 1992; Deramond et al. 1993; Roure & Combes 1998; Teixell 1998). Triassic and Jurassic aborted rifting events predated the development of a major Cretaceous crustal thinning event, which culminated in displacement between the Iberian and European plates (Puigdefàbregas & P. Souquet 1986; Vergés & Garcia-Senz 2001). Continental rifting in the Pyrenean domain occurred in response to the counterclockwise rotation of Iberia relative to Europe, coeval with the onset of oceanic spreading in the Bay of Biscay between Chron M0 and A33o (approximately 125-83 Ma) (Le Pichon et al. 1970; Choukroune & Mattauer 1978; Olivet 1996; Gong et al. 2008; Jammes et al. 2009). About forty metric- to kilometer-sized fragments of subcontinental mantle rocks are found along the northern flank of the Pyrenees, in the North Pyrenean Zone (NPZ). They reside within or next to numerous lozenge-shaped basins flanking the North Pyrenean Fault (NPF). These basins are interpreted as the remnants of isolated, pull-apart or transtensive half graben basins formed in response to the eastward drift of Iberia along the NPF and later inverted during the Late Cretaceous-Early Cenozoic

127 Pyrenean orogeny (Le Pichon et al. 1970; Choukroune & Mattauer 1978). A typical flysch
128 sedimentation started during the mid-Albian within these basins (black flysch), which later
129 enlarged during the Late Albian and connected into one single, wider basin trough during the
130 Cenomanian (Debroas 1976; P. Souquet et al. 1985; Debroas 1990).

131 Various scenarios have been proposed for the emplacement of the ultramafic bodies, ranging
132 from purely tectonic mechanisms, such as solid intrusion of hot or cold mantle rocks into
133 sediments during strike-slip events (Avé-Lallemand 1967; Minnigh et al. 1980; Vielzeuf &
134 Kornprobst 1984), to tectono-sedimentary processes in which mantle rocks were exhumed
135 during Variscan time (Mattauer & Choukroune 1974; Fortane et al. 1986) and reworked in a
136 mid-Cretaceous wild flysch (Fortane et al. 1986). In recent re-examinations, various authors
137 propose that some of these bodies are fragments of sub-continental mantle basement partially
138 exhumed during Albian-Cenomanian times (Lagabriele & Bodinier, 2008; Jammes et al.
139 2009; Lagabriele et al. 2010; Debroas et al. 2010; Clerc et al. 2012). Within the NPZ, the
140 metasediments are locally strongly deformed and underwent a High Temperature - Low
141 Pressure (HT-LP) mid-Cretaceous metamorphic event, which lasted nearly 30 Ma from 110
142 Ma to 80 Ma (Azambre & Rossy 1976; Albarède & Michard-Vitrac 1978b; Montigny et al.
143 1986; Golberg et al. 1986; Goldberg & Maluski 1988; Thiébaud et al. 1988; Thiébaud et al.
144 1992). This metamorphism is considered as a consequence of crustal thinning (Golberg &
145 Leyreloup 1990) and developed in relation with hydrothermal circulations (Dauteuil & Ricou
146 1989). Hydrothermal circulations are also responsible for extensive albitization of some of the
147 North Pyrenean Massifs (Demange et al. 1999; Boulvais et al. 2007; Poujol et al. 2010), and
148 formation of massive talc deposits (Moine et al. 1989; Schärer et al. 1999; Boulvais et al.
149 2006) probably in relation to the activity of major ductile extensive shear-zones (Passchier
150 1984; St Blanquat et al. 1986; Costa & Maluski 1988; St Blanquat et al. 1990; St Blanquat
151 1993).

152

153 **III. Geology of the sampling sites**

154 The ophicalcites and related ultramafic breccias selected for the oxygen and carbon isotope
155 study were sampled from peridotite bodies exposed all along the NPZ (fig. 1). We selected
156 nine localities which are representative of the variety of the Pyrenean peridotites, and
157 presumably of the different geological processes involved in their exhumation history. Two
158 sampling sites are located in the western Pyrenees (Urdach and Tos de la Coustette), one in
159 the central Pyrenees (Moncaup) and nine in the Eastern Pyrenees (Ercé-Angladure, Lherz,
160 Fontête Rouge, Freychinède, Berqué, Vicdessos, Urs, Bestiac, Caussou).

161

162 **III.1. Western peridotites**

163 Several peridotite bodies outcrop in the Chaînons Béarnais, within the fold and thrust belt
164 Mesozoic sequence of the NPZ, at a longitude corresponding to the western termination of the
165 Paleozoic Pyrenean axial zone. The base of the stratigraphic sequence, exposed along the
166 Mail Arrouy, Sarrance and Layens post-Cenomanian thrusts (Casteras 1970), is composed of
167 Late Triassic evaporites, breccias and ophites overlain by Mesozoic platform carbonates
168 forming the original cover of the northern Iberian margin (Canérot et al. 1978; Canérot &
169 Delavaux 1986). In contrast to the Eastern NPZ, evidence of HT-LP metamorphism is
170 restricted here to some scarce and narrow regions bordering fault contacts with Triassic and
171 mantle rocks (Fortane et al. 1986; Thiébaud et al. 1992; Lagabrielle et al. 2010) and the
172 temperatures during peak metamorphism barely exceeded 400°C (Clerc 2012). Petrological
173 and geothermobarometric studies of the western ultramafic bodies show that they underwent a
174 two step exhumation with a first rise from 60 km to 25 km depth (1050-950°C), probably
175 during late Hercynian times, followed by a further step from 25 km to a shallower and cooler

(600°C) level (Fabriès et al., 1998). This second step is marked by the development of a mylonitic fabric, from 117 Ma to 109 Ma (Vissers et al. 1997; Fabriès et al. 1998).

The Urdach body is a 1.5 km wide peridotite slice exposed at the western termination of the Mail Arrouy thrust (fig. 2A). It is overlain by Paleozoic basement slices and surrounded on its western and southern sides by a large volume of unsorted sedimentary breccias and olistoliths composed of peridotite fragments associated with Paleozoic basement clasts from upper, middle and lower crustal levels. These debris are intermingled in the Cenomanian black flysch (Casteras 1970; Vielzeuf 1984; Souquet et al. 1985; Jammes et al. 2009; Debroas et al. 2010). Some authors considered that the Urdach body itself might be an olistolith settled in Cenomanian sediments (Duée et al. 1984; Fortane et al. 1986). Peridotite hydrothermal alteration led to pervasive serpentinization reaching 80%. This is a dominant character of the Urdach body (Fabriès et al. 1998).

The 400 m long Tos de la Coustette ultramafic body is located 3 km west of the Sarailé summit, at the western termination of the Sarrance anticline (fig 2a). Apart from the peridotites, the faulted heart of the Sarrance anticline includes, Paleozoic basement rocks and ophite lenses embedded within cataclastic Triassic sediments. It is thrust over the verticalized Urgonian limestones and Albian flysch of the Lourdios Syncline (Casteras 1970; Lagabrielle et al., 2010). The Tos de la Coustette body itself is in tectonic contact with small lenses of Paleozoic crustal rocks and Triassic metaevaporites outcropping both above and beneath the peridotites. Like the Sarailé peridotites, the environment of the Tos de la Coustette body is devoid of sedimentary breccias; instead these bodies are entirely surrounded by cataclastic breccias limited by tectonic contacts and are thought never to have been exposed to the seafloor (Canérot & Delavaux 1986; Lagabrielle et al. 2010).

III.2. Central peridotites

The Moncaup ultramafic body is part of a group of peridotites exposures lying around the Milhas massif, in the central Pyrenees (fig. 1). They are associated with basement rocks, variably brecciated Triassic sediments, ophites and Albian mafic intrusions. They are overlain in tectonic contact by highly metamorphosed Mesozoic marbles (Debeaux & Thiébaud 1958; Hervouët et al. 1987; Barrère et al. 1984). Although the peridotites have risen to near surface levels, there is no evidence for sedimentary reworking indicating their exhumation on the basin floor. Indeed, based on their geological setting, it can be deduced that the mantle rocks have remained capped by the Mesozoic marbles together with small slices of continental crust, during their uplift along the detachment fault (Lagabrielle et al. 2010).

III.3. Eastern peridotites:

The eastern Pyrenean peridotites are found within narrow belts of Mesozoic sediments of the NPZ, mainly limestones, pinched between the Axial Zone to the south and blocks of Paleozoic crust to the North representing the continental basement of the NPZ (North Pyrenean massifs) (fig. 1). Although the eastern Pyrenean mantle outcrops are often small and disconnected from an original substratum, one can still observe, on a decametric scale, a progressive transition from carbonate-free massive peridotites to high carbonate content breccias with all intermediates. On the rim of the ultramafic bodies, the massive peridotites are often crosscut by millimetric to centimetric calcite veins over the first few meters. In addition, in many localities, the peridotites are reworked within sedimentary polymictic breccias together with highly variable proportions of carbonate clasts. The amount of matrix of these breccias increases toward the carbonated end-member.

Most of the ultramafic bodies sampled for this study, from West to East, namely Ercé-
Angladure, Lherz, Fontête Rouge, Freychinède, Berqué, Videssos, Urs, Bestiac and Caussou,
display geological settings consistent with an origin as olistoliths surrounded by polymictic
detritic formation (fig. 2B, 3). They are interpreted as sedimentary records of the exhumation
of the peridotites on the floor of the Cretaceous basins (Lagabrielle & Bodinier 2008; Clerc et
al. 2012). The ultramafic-bearing breccias show sedimentary features such as grain-sorting
and crossbeddings and can be found away from the main bodies, indicating that they have
been transported by sedimentary processes. Lagabrielle & Bodinier (2008) showed that the
polymictic ultramafic-carbonate clastic sediments have been emplaced into fissures opened
within the exhumed massive peridotites, in a way similar to OC2 sedimentary ophiolites of
Lemoine et al. (1987). Similar features are reported in more detail, together with the presence
of ultramafic-rich debris flows and evidence of ultramafic rock-fall in the vicinity of the
Lherz body by Clerc et al. (2012). The peridotites show little serpentinization, developed
mainly along discrete, localized joints and fissures. The carbonates reworked in the detritic
formations surrounding the peridotites are strongly deformed and underwent HT-LP
metamorphism with peak temperatures commonly as high as 600°C (Golberg & Leyreloup,
1990; Clerc 2012). By contrast to the western peridotites, the eastern ones underwent a single
and rapid uplift event, which probably limited hydrothermal alteration and serpentinization
(Albarède & Michard-Vitrac 1978a; Fabriès et al. 1991; Henry et al. 1998).

IV. Description of the analyzed samples

IV.1. Sampling strategy and collected samples

The sampling strategy was to collect samples from the four main geological environments
identified and distinguished as follows: (1) poorly serpentinized peridotites surrounded by hot

metasediments (Eastern and central peridotites) either exhumed to the basin floor (Lherz, Bestiac, Caussou, Vicdessos, Urs, Ercé-Angladure) or only unroofed but never exhumed (Moncaup), and (2) highly serpentinized peridotites surrounded by cooler sediments (Western peridotites) either exhumed to the basin floor (Urdach) or only unroofed but never exhumed (Tos de la Coustette). The list of the 48 studied samples is given in Table 1. We focused this study on the Lherz and Urdach bodies since they are among the largest mantle outcrops in the Pyrenees and because they represent two well-studied end-members in terms of their geological environment. Furthermore, these two localities offer better outcrop conditions compared with the smaller bodies poorly exposed in areas presenting important vegetal covering and rock alteration.

IV.2. Field and macroscopic aspects:

IV.2.a. Western Pyrenean Ophicalcites:

The western ophicalcites appear essentially as veins of calcite infilling fissures and fractures opened within the ultramafic rocks. The fractures present relatively constant and repeated orientations (fig. 4A). Particularly well observable in a quarry opened on the western side of the Urdach Iherzolite body, they were first described by Monchoux (1970) and later interpreted as typical ophicalcite textures by Jammes et al. (2009). These authors highlighted their similarities with structures observed within exhumed mantle in the Alps and drilled off Iberia (Manatschal 2004). They consist mainly in millimetric to decimetric veins of clear white calcite (fig. 4B). The thickest veins are actually constituted of an accumulation of numerous veins and veinlets separated by thin fragments of peridotite strapped from the rims.

At Tos de la Coustette, the ophicalcites also appear as a dense mesh of very fine veinlets and as a pervasive substitution of serpentine minerals by patches of carbonate, barely visible on a

macroscopic scale, invading highly serpentized peridotites (fig. 4C and D). Similar textures have also been described further east in the Avezac-Moncaut peridotites (Fabriès et al. 1998).

IV.2.b. Central Pyrenean Ophicalcites:

At least two types of ophicalcites were identified in the Moncaup peridotites. The first one, observed close to the damage zone of the tectonic contact between the peridotites and the overlying marbles, is represented by millimetric veins of coarse translucent sparite (fig. 4E). The veins crosscut and hence post-date a mylonitic fabric affecting the peridotites. The second one, observed in the damage zone of the detachment fault, consists of light brown micro-conglomerates and micrite infilling veins and cavities opened in the altered and dislocated peridotites (fig. 4F). The cavities present contorted and rounded rims. The micro-sediments show complex multi-generation evolutions with successive stages of deposition indicated by several color shades and crosscutting sparitic veins. The micro-conglomerates are laminated and present clear grain-sorting.

IV.2.c. Eastern Pyrenean Ophicalcites:

In the Eastern Pyrenees, ophicalcites and polymictic ultramafic-marble bearing breccias are observed within, close to, and even far away from the main peridotite bodies. Most of the clasts are composed either of ultra-fresh subcontinental peridotites or of marbles bearing mineral assemblages typical of the HT-LP mid-Cretaceous metamorphism. They are associated with a minor proportion of fragments deriving from gabbros, Triassic ophites Mesozoic meta-pelites and meta-evaporites and Paleozoic basement rocks (Lagabrielle & Bodinier 2008; Clerc et al. 2012).

In the Etang de Lherz area, Lagabrielle and Bodinier (1998) identified four main types of breccias and ophicalcites that can be extended to the other peridotite outcrops of the Eastern Pyrenees. (i) Type 1 is found in direct contact with or within the ultramafic body, it consists

294 of a carapace of monomictic breccias resulting from the cataclastic deformation of the
295 peridotites during exhumation. These breccias typically lack carbonate clasts and contain little
296 to no carbonate veins and cement. Therefore, they will not be considered further in this study.

297 (ii) Type 2 breccias, generally found in close contact with type 1 breccias, are ultramafic-
298 dominated polymictic breccias resulting from the sedimentary reworking of type 1. (iii) Type
299 3 breccias consist of thin layers of graded ultramafic litharenites bearing isolated cm-sized
300 clasts of peridotites and marbles and presenting slumps and syn-sedimentary normal faults
301 (fig. 5A and B). Within the type 3 breccias, the peridotite clasts display many different
302 lithologies (lherzolite, harzburgite, websterite, pyroxenite etc.), variable mantle textures
303 (equant coarse-granular to mylonitic) and variable degrees of serpentinization (totally fresh to
304 fully serpentinized, fig. 5C and D). These observations point to mixing and transport from a
305 relatively distant source by sedimentary processes. Furthermore, clasts of former monomictic
306 carbonate breccias and polymictic UM-marble breccia are also reworked in these formations,
307 pointing to their late deposition with regard to the exhumation history (Clerc et al., 2012). (iv)
308 Type 4 breccias correspond to clastic rocks closely resembling the OC2 sedimentary
309 opicalcites of Lemoine et al. (1987). Clear white calcite veins penetrate fractured ultramafic
310 blocks in which they separate angular fragments. There is a striking association of these veins
311 with matrix-supported microbreccias similar to those forming the matrix of the type 2 breccias
312 (fig. 5E). The veins are smoothly rooted in the matrix and seem to be its extension in narrow
313 domains where the clasts were too big to fit. However, some veins crosscut pre-existing
314 matrices, pointing to a contemporaneous formation of matrices and veins during
315 sedimentation accompanied by multi-stage circulations of cementing fluids. In some outcrops,
316 the ultramafic clasts exhibit a centimeter thick orange-brown oxidation ring on their contact
317 with carbonate matrices and veins (fig. 5 E and F). This feature is also commonly observed in
318 oceanic opicalcites (Boschi et al. 2006; Dick et al. 2008). This oxidation pattern does not

appear on the rims of the thinnest veins.

Ophicalcites at the Bestiac locality show similar features and offer exceptional conditions to investigate the successive generations of serpentinization and carbonation. The peridotite consists of tens of lens-shaped bodies less than a few hundred meters in size and embedded in a metamorphic bimodal ultramafic-marble breccia. Angular to slightly rounded centimeter-sized clasts of lherzolite are found more than 500 m away from the main blocks, a pattern clearly not consistent with any fault-assisted mode of emplacement. A few outstanding outcrops are visible in several abandoned caves and galleries dug for prospection of asbestos. Fresh to dark green serpentinites are crosscut by networks of cm-thick light green fibrous serpentine (likely chrysotile) delimitating metric lumps which mimict at a meter-scale the classical microscopic mesh-texture of serpentinized peridotites (Wicks & Whittaker 1977) (fig. 5G). The serpentine veins commonly show oblique sigmoidal fibers indicating shearing contemporaneous to brittle deformation responsible for vein development. Pluri-millimetric veins of calcite crosscut through this latest generation of serpentine veins that acted as a weak gateway for sediments and fluids during the ultimate stage of deformation and sedimentary reworking (fig. 5H). Some of the calcitic veins have a reddish coloration and increased concentration of oxides, suggesting possible syn- or post-diagenetic hydrothermal circulation. As in the Lherz area, these remarkable ultramafic-bearing formations have a relatively restricted extension and appear within large volumes of clastic formations devoid of any ultramafic component.

IV.3. Microscopic description:

Ophicalcite from the Urdach ultramafic body have millimetric veins of sparite. Several vein generations crosscut each other with varying angles. The calcite veins commonly show crack-

343 seal aspects. Symmetric layers of calcite with varying intensity in transmitted light and
344 cathodoluminescence (CL), induced by minor variations of composition or inclusion
345 concentration, are separated by a central suture (fig. 6A). Some of the largest veins actually
346 consist of an accumulation of numerous sub-parallel veinlets, less than a micrometer wide,
347 invading the serpentinite (fig. 6B). Finally, some other veins show zonated botryoids of
348 fibrous radiating calcite (fig. 6C)

349 In the Tos de la Coustette opicalcites, the carbonates mainly appear as micrometric to
350 millimetric patches of calcite extensively dispersed within the serpentinite (fig. 6D). Intimate
351 repartition of calcite and serpentine indicate a pervasive calcification by replacement of some
352 serpentinous phases. The poorly elongated calcite aggregates develop following a general
353 foliation marked by magnetite alignments and thin yellow serpentine veinlets. Surface
354 estimate by digital image treatment indicates that the rock includes up to 55 % calcite, 40 %
355 serpentine and 5 % magnetite with minor phases.

356 The matrix of the eastern Pyrenean opicalcites and associated polymictic breccias consists of
357 a pale-orange litharenite composed of infra-millimeter-sized angular clasts of marbles mixed
358 with varyingly serpentinized ultramafic clasts and isolated minerals (pyroxenes, olivine, green
359 and brown spinels). This litharenite sometimes appears laminated and shows graded-bedding
360 due to sedimentary transport (Lagabriele & Bodinier 2008; Clerc et al. 2012) (fig. 6E). In
361 contrast to the veins, the matrices of the breccias, show much less evidence for
362 recrystallization: there are, for example, a few newly formed metamorphic phyllosilicates and
363 amphiboles.

364 Most of the veins observed in the Eastern Pyrenean opicalcites consist of clear and equant
365 sparry calcites (fig. 6F). The veins cross cut alternatively the ultramafic clasts and the matrix
366 of the breccias in which they often seem to be rooted. In the simplest cases, a single

generation of calcite crystal nucleates from the rims of the veins and grows toward the center where it joins in a central suture. In some cases, the growth resumed or the fracture was reopened, leading to the formation of vugs. Most of the veins show multistep histories with successive infillings of sparite particularly well highlighted by varying luminescence in CL (fig. 6G). When pure enough, the veins are clearly recrystallized as evidenced by the conservation of former zoned calcite dogteeth ghosts within bigger equant neoformed crystals. The borders of the neoformed crystals are independent from those of the ghosts that they overprint (fig. 6H). When thick enough, the veins are generally filled with detrital material including micro-fragments of serpentine, oxides and calcite clasts mixed within a micrite. Although they lack microfossils, such veins resemble the neptunian dykes and veins formed on the subaquatic floor and consequently opened to sedimentary influx (Smart et al. 1987; Laznicka 1988; Winterer et al. 1991).

V. Methods for determination of O and C isotope compositions

Rock samples were sawed to select well-oriented and relevant planes. The sawed faces were cleaned using water and pulsed with dry air before micro-drilling. A minimum of about 20 mg of powder was collected for each sampling site.

The O and C isotope compositions were measured using a VG SIRA 10 triple collector mass spectrometer at the University of Rennes 1, on the CO₂ released during reaction of calcite with anhydrous H₃PO₄ in sealed vessels at 50°C (McCrea 1950). NBS 19 and internal-lab standard references materials (Prolabo Rennes) were continuously measured during the course of this work. NBS 19 measured values were $\delta^{18}\text{O} = 28.26 \pm 0.09$ (1 σ , n=12) ‰ and $\delta^{13}\text{C} = 1.86 \pm 0.02$ (1 σ , n=12) ‰. Results were corrected in accordance with the NBS 19 recommended values of 28.65‰ and 1.95‰, for O and C respectively. The analytical uncertainty is estimated at 0.15‰ and 0.1‰ for O and C.

VI. Results

The isotope compositions for the 48 analyzed samples are presented in table 1 and figure 7. The calcite phase found in clasts, veins and matrices from the Pyrenean ophicalcites and ultramafic-bearing breccias displays a wide range of oxygen isotope compositions with minimum values of 12.6 and 13.8‰ (vs. SMOW) measured in Moncaup and Tos de la Coustette veins (Western ophicalcites), and maximum values of 25.1‰ in the matrices of samples from Etang de Lherz area (fig. 4 & 6; Eastern ophicalcites). The carbon isotope compositions range from -5.8‰ (vs. PDB) in Moncaup samples to 1.5‰ in Lherz samples (matrices). As a whole, the field of isotopic compositions of Pyrenean ophicalcites is displaced from the one of the Iberian margin ophicalcites by lower $\delta^{18}\text{O}$ values and slightly lower $\delta^{13}\text{C}$ values (arrow in figure 7). Whereas no clear distinction can be made when comparing Pyrenean ophicalcites with Alpine and Apenninic ones, it seems that hydrothermal ophicalcite worldwide compare well with ophicalcites from the Western Pyrenees. First order analysis of the distribution of the oxygen and carbon isotope compositions implies to distinguish two separate domains: i) Ophicalcites from the Urdach and Tos de la Coustette ultramafic bodies have rather low and variable values of $\delta^{18}\text{O}$ and $\delta^{13}\text{C}$, ranging from $\delta^{18}\text{O} = 13.8$ to 22.1 ‰ and $\delta^{13}\text{C} = -5.22$ to 1.12 ‰ and scattered around a mean value of $\delta^{18}\text{O} = 19.1$ ‰ and $\delta^{13}\text{C} = -1.0$ ‰. Ophicalcites from Tos de la Coustette body plot into a distinct field having an extremely low value of $\delta^{18}\text{O}$. ii) Ophicalcites from the Eastern Pyrenean bodies display low dispersion (21.3 to 25.1 ‰) in $\delta^{18}\text{O}$ but variable $\delta^{13}\text{C}$ values (1.53 to -2.47 ‰). Among the Eastern Pyrenean ophicalcites, very poor discrimination can be made based on the composition of veins and matrices since both display almost similar values with mean $\delta^{18}\text{O}$ of 23.4 ‰ in the veins and 24.1 ‰ in the matrices. The O and C isotope compositions of the nine samples containing both veins and matrices are reported in figure 8. One can observe good correlations between the compositions of matrices and veins with the exception of samples

LHZ8 and LHZ64 whose veins are significantly depleted in ^{18}O and slightly enriched in ^{13}C . We note that the pluri-millimetric size of our sampling drilling spots provide bulk estimates of the isotopic compositions of the veins and matrix but do not allow the complex multistage history recorded in some of the veins to be deciphered (i.e. fig. 6G). The isotope composition of the matrices does not correlate with the variable lithology of the clasts (either ultramafic and/or carbonate), nor with the relative amount of clasts. In contrast the isotopic compositions of the marble clasts are highly variable and plot within a larger field than the matrices and veins (Fig. 7). Also, there is no correlation between the isotopic compositions of clasts and the veins or matrices that host them. Actually, these clasts underwent a strong HT/LP metamorphism and may contain abundant silicates (phyllosilicates, amphiboles, scapolite). Closed-system isotopic equilibration between the carbonate and the silicate phases likely introduced variable isotopic alteration of the carbonate phase, depending on the initial amount of detrital silicates in the sedimentary precursor (see for example Valley, 1986; Boulvais et al., 2000). Also, open-system alteration during syn-metamorphic infiltration possibly caused isotopic shifts, which remain difficult to estimate here because we have no more information on the initial geometry of the clast (for example the distance to a lithological discontinuity). The ophicalcites from the Moncaup body display two distinct generations of carbonates with distinct isotopic compositions (fig. 4C and D). Such differences in isotopic compositions are consistent with the occurrence of two types of textures as described in section IV.

VII. Discussion

VII.1. Origin of the various types of ophicalcites

Based on the petrographic descriptions on the one hand and on the stable isotope compositions on the other, we are able to distinguish three main categories of ophicalcites associated with the subcontinental mantle bodies of the northern Pyrenees (table 2).

The first type of ophicalcites or *hydrothermal type*, as defined in the Tos de la Coustette body results from peridotite carbonation by veins and pervasive substitution of the serpentinite minerals by low $\delta^{18}\text{O}$ calcite. The low $\delta^{18}\text{O}$ values of calcite indicate that carbonation occurred from rather hot fluids. Comparable $\delta^{18}\text{O}$ values have been measured in ophicalcites formed in oceanic and ophiolitic hydrothermal systems (Lavoie & Cousineau 1995; Artemyev & Zaykov 2010). Due to its low $\delta^{18}\text{O}$, the first generation of coarse crystalline calcite veins described in the Moncaup peridotite likely corresponds to this type of hydrothermal ophicalcite. The difference in texture types between the Moncaup and the Tos de la Coustette ophicalcites may be explained by the very different rheology and chemical response to fluid circulation of the unserpentinized peridotite at Moncaup compared with the totally serpentinized peridotite of Tos de la Coustette.

The second type of ophicalcites or *tectonically-controlled type* is well characterized in the Urdach body. It consists of massive serpentinized peridotites, indifferently lherzolite or harzburgite, crosscut by successive generations of millimetric to centimetric calcite veins with intermediate isotopic compositions. The tectonic control of calcite crystallization is documented by the distribution of veins along preferential planes and their crack-seal geometry. Such calcite crystallizations likely record the arrival of the peridotite close to seafloor environments, directly under the influence of waters with intermediate temperature. Different generations of veins cross-cutting each other with slight variations in isotopic composition may reflect some temperature variations during the successive steps of fracturing / precipitation. In sample URD 1, a first generation of vein with a lower $\delta^{18}\text{O}$ values ($\delta^{18}\text{O}=18.6\text{‰}$) is cut by a later generation with a higher $\delta^{18}\text{O}$ value ($\delta^{18}\text{O}=21.1\text{‰}$). This is

consistent with cooling during vein formations, in consequence of progressive exhumation, provided that the isotopic composition of the invading fluid, and then its source, remained constant throughout the history of this sample.

The third type of ophicalcites, dominant in the eastern Pyrenees, is *sedimentary ophicalcite*. It consists of a cogenetic association of calcite vein and polymictic breccias. The matrix-supported to clast-supported polymictic breccias are composed of variable proportions of marbles and UM clastic material. Polymictic compositions and typical sedimentary features such as grain-sorting and cross bedding indicate that these ophicalcites have a sedimentary origin (Clerc et al., 2012). Their wide lithological variety, both in UM and metasedimentary material, likely results from sedimentary transport and mixing. By analogy with neptunian veins observed in other extensional settings (Winterer et al. 1991), the micrite-filled brittle fractures have been interpreted as very late, near surface fracturing of the exposed ultramafic basement (Lagabriele & Auzende 1982; Morgan & Milliken 1996), possibly leading to gravitational instabilities: slumping, slope failure, and landslides as described at ODP site 899 by Gibson et al. (1996). The sparite-filled veins and veinlets, either reworked in the breccias, smoothly rooted in the matrix or crosscutting clasts and matrix reveal a multistage deposition history, already implied by the presence of breccias clasts reworked in the breccias (Clerc et al. 2012). Bernoulli & Weissert (1985) describe similar cogenetic and simultaneous sediment infillings and calcitic cement precipitation in Alpine ophicalcites. Such fractures must have allowed the circulation of sedimentary fluids or early diagenetic fluids in domains where restricted dimension hindered the penetration of sedimentary material. The isotopic compositions of matrices and veins (Fig. 8) show a good correlation in both the oxygen and carbon systems, which confirm the idea that both features developed from the same reservoir. Since the relationship is valuable on a rather large range of $\delta^{18}\text{O}$ and $\delta^{13}\text{C}$, one can infer that

the system of vein + matrix development was not connected to an external reservoir which would have produced veins with distinct compositions from the ones of the matrices.

Precipitation of acicular aragonite has commonly been correlated with warm water temperatures, high Mg/Ca ratios, high salinity, and high carbonate concentrations, conditions reached in the uppermost levels of serpentine seamounts (Haggerty 1987; Lagabriele et al. 1992). Similar thermal and chemical conditions are associated with fibrous, botryoidal calcite occurrences (Folk 1974; Surour & Arafa 1997), and botryoidal calcite could also represent a replacement texture of acicular radiating aragonite (Ross 1991). More equant and bladed sparry calcite has been correlated with cooler, deeper marine or meteoric settings, typically with low Mg, and carbonate concentrations (Folk 1974; Burton & Walter 1987). Instead, geochemical data (trace element and isotopic signatures) from Iberian margin ophicalcites indicate a seawater imprint at temperatures of 10-20°C, consistent with an early Cretaceous seawater only slightly modified by interaction with serpentinized peridotite basement (Milliken & Morgan 1996). For that reason, Morgan & Milliken (1996) suggested that the temporal evolution in the carbonate phase and morphology, from precipitation of aragonite, followed by fibrous, botryoidal calcite and finally to coarse, bladed sparry calcite may be controlled primarily by fluid flow rates through the vein rather than by variations of the chemical and thermal parameters (fig. 9).

The low temperature ophicalcites from the Moncaup body (MP84a, b, c) are peculiar in that they have extremely low $\delta^{13}\text{C}$ (< -5.00 ‰), indicative of interaction with organic material. Such carbon isotope compositions are commonly observed in karstic or calcrete precipitations from continental/meteoric waters transiting through soils and vegetation. These peculiar ophicalcites are located immediately below the cataclastic formations staking out the detachment fault between the peridotites and the overlying marbles. Due to the solubility and permeability contrast between these two formations, this interface is prone to concentrating

groundwater. However, we cannot specify if the formations observed are contemporaneous of any very early exhumation of the mantle rocks to subaerial (onland) environments in the Cretaceous or if they result from a later karstification and/or replacement of pre-existing ophicalcarbonates. Regardless the exact explanation, these values strongly differ from the rest of our dataset by a clear shift toward lower $\delta^{13}\text{C}$ values, allowing the distinction to be made between a surface-derived cement precipitated in karstic environments and sedimentary ophicalcites deposited in subaqueous conditions.

VII.2. Environmental conditions for the formation of Central and Eastern Pyrenean ophicalcites

The isotopic compositions of the Pyrenean ophicalcites fall into the same field as other ophicalcites from the literature (fig. 7). Only the three samples from Moncaup MP84a, b, and c are out of this range because of their low carbon composition indicative of interactions with carbon from soils, as discussed above. Ophicalcites from the Alps and Apennine were interpreted as having been formed by interaction with seawater moderately heated to 80 to less than 200°C (Barbieri et al. 1979; Barrett & Friedrichsen 1989; Früh-Green et al. 1990; Schwarzenbach 2011) or by sedimentary fluids later re-equilibrated during Alpine metamorphism (Weissert & Bernoulli 1984; Barbieri et al. 1979).

Samples from the Eastern Pyrenees are clearly recognized as sedimentary ophicalcites by their textures. Consistently, the Eastern Pyrenean ophicalcites have the highest $\delta^{18}\text{O}$ values measured in our sample set, a feature which is indicative of low temperatures of precipitation at near surface conditions. However, we notice a major difference in the oxygen isotope composition with ophicalcites from the Iberian margin (Agrinier et al. 1988; Evans & Baltuck 1988; Agrinier et al. 1996; Milliken & Morgan 1996; Plas 1997; Skelton & Valley 2000). Indeed, in the Iberian ophicalcites, which precipitated from low temperature seawater, the

536 $\delta^{18}\text{O}$ values of calcite are around 31‰ with $\delta^{13}\text{C}$ values varying between -1.7 and 2.2‰.
537 Instead, the Eastern Pyrenean sedimentary opicalcites analyzed in our study have
538 significantly lower $\delta^{18}\text{O}$ values (around 24‰) with carbon isotope compositions ranging from
539 -2.5 to 1.4‰, so that even if the envelope of Pyrenean sedimentary opicalcites mimic the
540 Iberian margin ones, it is displaced in the $\delta^{13}\text{C}$ vs. $\delta^{18}\text{O}$ space (grey arrow, fig. 7). At least,
541 three hypotheses can be proposed in order to explain these differences (fig. 10).

542 1. Lowering of the O and C isotope compositions could result from a metamorphic imprint
543 with introduction of externally-derived fluids. Isotopic exchanges between neoformed calcites
544 and the mineral silicates, mainly serpentinite, which form a significant portion of the detrital
545 material associated with the sedimentary opicalcites, may lower the O isotope composition
546 of the calcite. The breccias and opicalcites rework clasts of pre-rift material that already bear
547 signs of high-grade recrystallization during the regional HT/LP metamorphism, with the
548 development of scapolite and amphibole. The deposition of the breccias and opicalcites
549 hence occurs after the peak of metamorphism. But the long-lasting mid-cretaceous thermal
550 anomaly is followed by a lower grade metamorphism that affects the Turonian-Senonian post-
551 rift sediments, with a maximum temperature near 350°C (Ternet et al., 1997; Clerc 2012).
552 This later and lower grade metamorphism may hence have affected the opicalcites and
553 breccias presented in this study. However, the petrographical effect of metamorphism on
554 these rocks seems rather limited since the matrices show only little recrystallization.
555 Furthermore, we would expect that the oxygen isotope composition would be much more
556 variable depending on the fluid/rock ratio. This is the case for a metamorphic-driven
557 alteration of the isotopic signal as shown from the study of the Alpine opicalcites (Fig. 7;
558 Weissert & Bernoulli 1984; Früh-Green et al. 1990). Also, one would have expected that the
559 veins show more constant composition instead of displaying delta values that correlate with
560 the values of matrices (Fig. 8).

2. The low O and C compositions may be the result of a hot diagenesis from marine porewater during carbonation. This hypothesis, which implies active circulation of relatively hot fluids in the boundary layer between the ultramafic basement and seawater, is consistent with the high geothermal gradients known to characterize the basins of the North Pyrenean Zone during the Albian-Cenomanian period (Dauteuil & Ricou 1989; Golberg & Leyreloup 1990). The thermal gradients for the Albo-Cenomanian metamorphism can be higher than 100°C/km. In such conditions, we may also consider that unconsolidated sediments still soaked with seawater can be rapidly buried and heated to temperatures as high as 50-80°C. At such temperatures, the calcite precipitated from seawater ($\delta^{18}\text{O} = 0\text{‰}$) would have a $\delta^{18}\text{O}$ value of around 23‰ (considering the isotopic fractionation coefficient of Zheng, 2011), a value that compares well with the data of the Eastern ophicalcites. Thermal gradients as high as 160-180°C/km are known in present days, for instance in the Salton Sea geothermal field (Elders et al., 1972; Muffler & White, 1969). Comparable environments can also be found on the top of mantle exhumed in oceanic domains, where hydrothermal fields develop over areas several square kilometerswide (around 2.5km² at the Rainbow hydrothermal site, German et al., 1996; around 2km² at the Lost City hydrothermal site, Kelley et al., 2001, along the Mid-Atlantic Ridge). In similar settings, in the ophiolites of East Liguria, Spooner and Fyfe (1973) describe temperatures as high as 400°C for shallow depth of circa 300 m below the water/rock interface.

3. As a last hypothesis, it may be that the Eastern Pyrenean sedimentary ophicalcites formed in a low-temperature but endorheic environment, dominated by continental waters and possibly disconnected from the ocean. Indeed, the oxygen composition measured here is about 7‰ lower than the present-day marine Iberian ophicalcites, a difference consistent with the difference between marine and unspecific waters with a continental affinity. Note first that a continental environment is not precluded by the existence of marine fauna, which would

have been observed in sediments associated with opicalcites. The hypothesis of an endorheic environment dominated by continental waters has to be questioned with respect to the paleogeographic reconstructions of the Pyrenean realm during mid-Cretaceous times. These reconstructions point to the existence of a V-shape opening oceanic domain, narrowing from the Bay of Biscay toward the East where it propagates into the continental crust (Jammes et al. 2009 and references therein). The opening of numerous transtensive basins of limited extension in the central and eastern part of the pre-Pyrenean domain may have been such that these basins were endorheic (Le Pichon et al. 1970; Choukroune & Mattauer 1978), partially disconnected from a marine influence at the time of opicalcite development. This hypothesis is consistent with the stratigraphy of the Albian sediments deposited in disconnected basins separated by positive reliefs (Debroas, 1976, 1990; Souquet et al., 1985). Some of these reliefs such as the future North Pyrenean massifs and the future Axial Zone were emerged, as shown by the outline of the Cenomanian transgression and by evidence of cooling and sedimentary reworking of crustal material (Filleaudeau et al., 2011). Such short wave-length and high amplitude morphology likely resulted from the flexural response of the lithosphere to the extreme crustal stretching due to the extensional Albian-Cenomanian tectonics along the Pyrenean realm. In such conditions, we may envision that the area where mantle has been exhumed was surrounded by subaerial catchments and, at that time possibly disconnected from the sea. A possible present-day analog is represented by the Salton Sea basin, which is an endorheic continental basin located ahead of the propagating oceanic spreading axis of the Gulf of California. Circulations of continental waters within sediments are also described in more opened environments, for example at the foot of the Aden Gulf margins (Lucazeau et al. 2010).

At this time, it is difficult to select between the three hypotheses even if the last one is the simplest in term of the isotopic composition record. Additional informations like fluid

inclusion data is needed to strengthen this hypothesis. It remains clear that, regardless of the exact explanation, sedimentary opicalcites in the Eastern Pyrenees are distinguishable from those in the Central and in the Western Pyrenees.

VII.3. Western and Eastern Pyrenean opicalcites: why are they so different?

The three types of opicalcites identified in this study have to be considered within the frame of the exhumation history of the Pyrenean peridotites presented in section III a and c and as summarized in figure 11. We highlight a clear distinction between the Eastern and Western Pyrenean isotope composition of opicalcites also evidenced by the different degrees of serpentinization of the mantle that host them, by the temperatures of the metamorphic peak in the surrounding metasediments (Choukroune & Seguret, 1973; Golberg & Leyreloup, 1990; Ravier, 1959; Clerc 2012) and by the typologies of opicalcites (fig. 11). Following our observations, and in accordance with phase stability of serpentine mineral (Andreani et al. 2007), it appears that the variable serpentinization degree of the Pyrenean peridotites can be linked, primarily, to the thermal anomaly accompanying their exhumation. Since carbonation postdated serpentinization, the degree of serpentinization appears as a key factor influencing the development of opicalcites. Volume increase and rheological softening induced by serpentinization tend to favor the development of numerous fractures, allowing an endogenic precipitation of carbonates as observed in the Western opicalcites. In contrast, the less serpentinized peridotites exposed in Moncaup and in the Eastern Pyrenees must have had a different behavior during uprising to crustal levels. Their contrasting rheology with the surrounding rocks implies that they were probably still massive and competent until exhumation. This could explain the predominance of superficial opicalcites found in these localities. The fact that the Eastern Pyrenean peridotites remained preserved from hydrothermal circulation may explain their scarce serpentinization. In addition, such a lack of fluid activity may also be responsible for the preservation of high temperature mineral

assemblage since heat was evacuated by convection. The reason of the limited access of fluids to the exhuming peridotites is not yet understood. We could suggest either i) a blanketing effect of the Mesozoic sedimentary cover that would inhibit water infiltration, or ii) fast exhumation in a continental environment with limited amounts of water available for hydrothermal circulations.

Conclusion

On the basis of close fieldwork, petrographic and geochemical considerations, we present the first comprehensive review of the Pyrenean opicalcites. Our results, in accordance with published studies on worldwide occurrences of opicalcites allowed us to distinguish and characterize three main types of opicalcite (table 2): (i) hydrothermal opicalcites resulting in low $\delta^{18}\text{O}$ calcite (13.8‰) pervasively replacing serpentinite; (ii) intermediate or syn-tectonic opicalcites developed along with brittle discontinuities in the serpentinitized mantle rocks, with intermediate calcite isotope compositions ($\delta^{18}\text{O}$ around 20.0‰; $\delta^{13}\text{C}$ around -1.06‰); (iii) sedimentary opicalcites occurring as breccias and neptunian dykes, associated with the circulation of syn-sedimentary fluids. The isotopic compositions for this sedimentary type show the highest $\delta^{18}\text{O}$ and $\delta^{13}\text{C}$ values of the set, consistent with the cold temperatures of precipitation expected in a sedimentary environment. We note a non-linear distribution of the different opicalcite type along the Pyrenean range, with dominant endogenic ones in the West and dominant exogenic ones in the East. Such a distribution is clearly linked to a difference in serpentinitization degrees likely related to the different exhumation histories and subsequent variable thermal anomalies.

We further investigated the possible origins of the fluid and temperatures at which the calcite may have precipitated in both hydrothermal and sedimentary domains. We present three

660 possible explanations for the relatively low values of the sedimentary ophicalcites: i) a post-
661 sedimentary metamorphic imprint; ii) a hot diagenesis in relation to the high regional thermal
662 gradient; iii) sedimentation in an endorheic basin. This last hypothesis is consistent with the
663 paleogeographic reconstructions of isolated Albo-Cenomanian basins at the tip of a
664 propagating rift. Finally, we highlight a major difference between Eastern and Western
665 ophicalcites, linked primarily to the variable degree of serpentinization. Considering the
666 strong control of serpentinization on the rheology of mantle rocks we propose that the
667 formation of different ophicalcites types is controled by the degree of serpentinization,
668 depending itself on the rate and modalities of exhumation of the subcontinental mantle during
669 extreme crustal stretching.

670

Acknowledgments:

This work was made possible thanks to CNRS, Total, and the Action Marges research group (INSU, Total, IFP, BRGM, IFREMER) through a Ph.D. grant to C. Clerc. We thank G. Frühgreen and G. Manatschal for their valuable comments that helped improve the quality of the manuscript. We are grateful to B. Smith for improving the English, to J. -C. Ringenbach and Benoit Ildefonse for fruitful discussions and improvement on the quality of the figures, and to C. Nevado for the high quality thin-sections realized at the Géosciences Montpellier laboratory.

References

- Abbate, E., Bortolotti, V., & Passerini, P. (1970). Olistostromes and olistoliths. *Sedimentary Geology*, 4(3-4), 521-557. doi:10.1016/0037-0738(70)90022-9
- Agrinier, P., Cornen, G., & Beslier, M. O. (1996). Mineralogical and oxygen isotopic features of serpentinites recovered from the ocean/continent transition in the Iberia abyssal plain. In R. B. Whitmarsh, D. S. Sawyer, A. Klaus, & D. G. Masson (Éd.), *Proceedings of the Ocean Drilling Program, 149 Scientific Results* (Vol. 149, p. 541-552). Ocean Drilling Program.
- Agrinier, P., Mével, C., & Girardeau, J. (1988). Hydrothermal Alteration of the Peridotites Cored at the Ocean/Continent Boundary of the Iberian Margin: Petrologic and Stable Isotope Evidence. In G. Boillot, E. L. Winterer, & et al. (Éd.), *Proceedings of the Ocean Drilling Program, 103 Scientific Results* (Vol. 103, p. 225-234). Ocean Drilling Program. Consulté de http://www-odp.tamu.edu/publications/103_SR/103TOC.HTM
- Albarède, F., & Michard-Vitrac, A. (1978a). Datation du métamorphisme des terrains secondaires des Pyrénées par des méthodes Ar-Ar et Rb-Sr. Ses relations avec les péridotites associées. *Bulletin de la société géologique de France*, XX(7), 681-688. doi:10.1016/0012-821X(78)90157-7
- Albarède, F., & Michard-Vitrac, A. (1978b). Age and significance of the North Pyrenean metamorphism. *Earth and Planetary Science Letters*, 40(3), 327-332. doi:10.1016/0012-821X(78)90157-7
- Andreani, M., Mével, C., Boullier, A.-M., & Escartín, J. (2007). Dynamic control on serpentine crystallization in veins: Constraints on hydration processes in oceanic peridotites. *Geochemistry Geophysics Geosystems*, 8(2). doi:10.1029/2006GC001373

707 Artemyev, D. A., & Zaykov, V. V. (2010). The types and genesis of ophicalcites in Lower
 708 Devonian olistostromes at cobalt-bearing massive sulfide deposits in the West
 709 Magnitogorsk paleoisland arc (South Urals). *Russian Geology and Geophysics*, **51**(7),
 710 750-763. doi:10.1016/j.rgg.2010.06.003

711 Avé-Lallemand, H. G. A. (1967). Structural and petrofabric analysis of an « Alpine type »
 712 peridotite: The lherzolite of the French Pyrénées. *Leidse Geol. Meded.*, **42**, 1-57.

713 Azambre, B., & Rossy, M. (1976). Le magmatisme alcalin d'âge crétacé dans les Pyrénées
 714 occidentales; ses relations avec le métamorphisme et la tectonique. *Bulletin de la*
 715 *société Géologique de France*, **7**(18), 1725-1728.

716 Bailey, E. B., & McCallien, W. J. (1960). Some Aspects of the Steinmann Trinity, Mainly
 717 Chemical. *Quarterly Journal of the Geological Society*, **116**(1-4), 365 -395.
 718 doi:10.1144/gsjgs.116.1.0365

719 Barbieri, M., Masi, U., & Tolomeo, L. (1979). Stable isotope evidence for a marine origin of
 720 ophicalcites from the north-central Apennines (Italy). *Marine Geology*, **30**(3-4), 193-
 721 204. doi:10.1016/0025-3227(79)90015-X

722 Barrère, P., Bouquet, C., Debroas, E.-J., Péliissonier, H., Peybernès, B., Soulé, J.-C., Souquet,
 723 P., et al. (1984). Carte géol. France (1/50 000), feuille Arreau (1072). Orléans.

724 Barrett, T. J., & Friedrichsen, H. (1989). Stable isotopic composition of atypical ophiolitic
 725 rocks from east Liguria, Italy. *Chemical Geology: Isotope Geoscience section*, **80**(1),
 726 71-84. doi:10.1016/0168-9622(89)90049-3

727 Bernoulli, D., & Weissert, H. (1985). Sedimentary fabrics in Alpine ophicalcites, **South**
 728 Pennine Arosa zone, Switzerland. *Geology*, **13**(11), 755-758. doi:10.1130/0091-
 729 7613(1985)13<755:SFIAOS>2.0.CO;2

730 Bogoch, R. (1987). Classification and genetic models of ophicarbonates rocks. *Ophioliti*, **12**, 23-
 731 36.

732 Bonatti, E., Emiliani, C., Ferrera, G., Honnorez, J., & Rydell, H. (1974). Ultramafic carbonate
 733 breccias from the equatorial Mid-Atlantic Ridge. *Marine Geology*, 16, 83-102.
 734 Bonney, T. G. (1879). Notes on some Ligurian and Tuscan serpentinites. *Geol. Mag.*, 6(2),
 735 362-371.
 736 Bortolotti, V., & Passerini, P. (1970). Magmatic activity. *Sedimentary Geology*, 4(3-4), 599-
 737 624. doi:10.1016/0037-0738(70)90024-2
 738 Boschi, C., Früh-Green, G., Delacour, A., Karson, J. A., & Kelley, D. S. (2006). Mass transfer
 739 and fluid flow during detachment faulting and development of an oceanic core
 740 complex, Atlantis Massif (MAR 30°N). *Geochemistry Geophysics Geosystems*, 7, 39
 741 PP. doi:2006 10.1029/2005GC001074
 742 Boulvais P, Fourcade S, Gruau G, Moine B, Cuney M (1998) Persistence of premetamorphic
 743 C and O isotopic signatures in marbles subject to Pan-African granulite-facies
 744 metamorphism and U-Th mineralization (Tranomaro, southeast Madagascar)
 745 *Chemical Geology*, 150, 247-262.
 746 Boulvais P, de Parseval P, D'Hulst A, Paris P (2006) Carbonate alteration associated with
 747 talc-chlorite mineralization in the eastern Pyrenees, with emphasis on the St.
 748 Barthelemy Massif. *Mineralogy and Petrology*, 88, 499-526.
 749 Boulvais, P., Ruffet, G., Cornichet, J., & Mermet, M. (2007). Cretaceous albitization and
 750 dequartzification of Hercynian peraluminous granite in the Salvezines Massif (French
 751 Pyrénées). *Lithos*, 93(1-2), 89-106. doi:10.1016/j.lithos.2006.05.001
 752 Brotzu, P., Ferrini, V., Masi, U., Morbidelli, L., & Turi, B. (1973). Contributo alla conoscenza
 753 delle « Rocce Verdi » dell'Appennino centrale. Nota III. La composizione isotopica
 754 della calcite presente in alcuni affioramenti di oficalciti del F 129 (S. Fiora) e sue
 755 implicazioni petrologiche. *Period. Mineral.*, 42, 591-619.

756 Brun, J. P., & Beslier, M. O. (1996). Mantle exhumation at passive margins. *Earth and*
757 *Planetary Science Letters*, 142(1-2), 161-173. doi:10.1016/0012-821X(96)00080-5

758 Burton, E. A., & Walter, L. M. (1987). Relative precipitation rates of aragonite and Mg calcite
759 from seawater: Temperature or carbonate ion control? *Geology*, 15(2), 111-114.
760 doi:10.1130/0091-7613(1987)15<111:RPROAA>2.0.CO;2

761 Canérot, J., & Delavaux, F. (1986). Tectonic and sedimentation on the north Iberian margin,
762 Chaînons Béarnais south Pyrenean zone (Pyrenees basco-béarnaises)—New data about
763 the signification of the lherzolites in the Sarailé area. *Comptes Rendus de l'Académie*
764 *des Sciences - Series II*, 302(15), 951-956.

765 Canérot, J., Peybernès, B., & Ciszak, R. (1978). Présence d'une marge méridionale à
766 l'emplacement des Chaînons Béarnais (Pyrénées basco-béarnaises). *Bulletin de la*
767 *société Géologique de France*, 7(20), 673-676.

768 Casteras, M. (1970). Carte géol. France (1/50 000), feuille Oloron-Sainte-Marie (XV-46).
769 Orléans.

770 Choukroune, P., et M. Séguret. 1973. « Carte structurale des Pyrénées ». ELF-ERAP.

771 Choukroune, P., & ECORS Team. (1989). The Ecors Pyrenean deep seismic profile reflection
772 data and the overall structure of an orogenic belt. *Tectonics*, 8(1), PP. 23-39.
773 doi:198910.1029/TC008i001p00023

774 Choukroune, P., & Mattauer, M. (1978). Tectonique des plaques et Pyrénées: Sur le
775 fonctionnement de la faille transformante nord-Pyrénéenne; comparaisons avec les
776 modèles actuels. *Bulletin de la société géologique de France*, 20, 689-700.

777 Clerc, C., Lagabriele, Y., Neumaier, M., Reynaud, J.-Y., & St Blanquat, M. (2012).
778 Exhumation of subcontinental mantle rocks: evidence from ultramafic-bearing clastic
779 deposits nearby the Lherz peridotite body, French Pyrenees. *Bulletin de la Société*
780 *Géologique de France*.

781 Clerc, C., Lagabrielle, Y., Vauchez, A., Lahfid, A., Bousquet, R., Dautria J.-M., Labaume, P.
 782 (in prep.).

783 Clerc, C. 2012. « Evolution du domaine Nord-Pyrénéen au Crétacé. Amincissement crustal
 784 extreme et thermicité élevée: un analogue pour les marges passives ». PhD Thesis,
 785 Paris, France: Université Paris 6. <http://tel.archives-ouvertes.fr/tel-00787952>

786 Cornelius, H. P. (1912). Petrographische untershungen in den Bergen Zwischen Septiner -
 787 und Julierpass. *Diss. N. Jahr. Min.*

788 Cortesogno, L., Galbiati, B., & Principi, G. (1981). Descrizione dettagliata di alcuni
 789 caratteristici affioramenti di breccie serpentiniche della Liguria orientale ed
 790 interpretazione chiave geodinamica. *Ophioliti*, 6, 47-76.

791 Costa, S., & Maluski, H. (1988). Use of the ⁴⁰Ar-³⁹Ar stepwise heating method for dating
 792 mylonite zones: An example from the St. Barthélémy massif (Northern Pyrenees,
 793 France). *Chemical Geology: Isotope Geoscience section*, 72(2), 127-144.
 794 doi:10.1016/0168-9622(88)90061-9

795 Dauteuil, O., & Ricou, L. E. (1989). Une circulation de fluides de haute température à
 796 l'origine du métamorphisme crétacé nord-Pyrénéen. *Geo*, 3(3), 237-250.

797 Debeaux, M., & Thiébaud, J. (1958). Les affleurements du socle paléozoïque entre les massifs
 798 de la Barousse et de Milhas. *Bull. Soc. Hist. Nat. Toulouse*, 93, 522-528.

799 Debroas, E.-J. (1976). Sédimentogenèse et position structurale des flyschs crétacés du versant
 800 nord des Pyrénées centrales. *Bull. Bur. Rech. Géol. Min.*, 1(4), 305-320.

801 Debroas, E.-J. (1990). Le flysch noir albo-cenomanien témoin de la structuration albienne à
 802 sénonienne de la Zone nord-pyrénéenne en Bigorre (Hautes-Pyrénées, France).
 803 *Bulletin de la société Géologique de France*, 8(2), 273-285.

804 Debroas, E.-J., Canérot, J., & Billotte, M. (2010). Les brèches d'Urdach, témoins de
 805 l'exhumation du manteau pyrénéen dans un escarpement de faille vraconnien-

cénomaniens inférieurs (zone nord-pyrénéenne, Pyrénées-Atlantiques, France). *Géologie de la France*, 2, 53-63.

Demange, M., Lia-Aragnoet, F., Pouliguen, M., Perrot, X., & Sauvage, H. (1999). Les syénites du castillet (massif de l'agly, Pyrénées orientales, France): une roche exceptionnelle dans les Pyrénées. *Comptes Rendus de l'Académie des Sciences - Series IIA - Earth and Planetary Science*, 329(5), 325-330. doi:10.1016/S1251-8050(00)88582-1

Demeny, A., Vennemann, T., & Koller, F. (2007). Stable isotope compositions of the Penninic ophiolites of the Kőszeg-Rechnitz series. *Central European Geology*, 50(1), 29-46. doi:10.1556/CEuGeol.50.2007.1.3

Deramond, J., Souquet, P., Fondecave-Wallez, M.-J., & Specht, M. (1993). Relationships between thrust tectonics and sequence stratigraphy surfaces in foredeeps: model and examples from the Pyrenees (Cretaceous-Eocene, France, Spain). *Geological Society, London, Special Publications*, 71(1), 193-219. doi:10.1144/GSL.SP.1993.071.01.09

Dick, H. J. B., Tivey, M. A., & Tucholke, B. E. (2008). Plutonic foundation of a slow-spreading ridge segment: Oceanic core complex at Kane Megamullion, 23°30'N, 45°20'W. *Geochemistry Geophysics Geosystems*, 9, 44 PP. doi:2008.10.1029/2007GC001645 [Citation]

Dietrich, V., Vuagnat, M., & Bertrand, J. (1974). Alpine metamorphism of mafic rocks. *Schweizerische Mineralogische und petrographische Mitteilungen*, 54, 291-323.

Duée, G., Lagabrielle, Y., Coutelle, A., & Fortané, A. (1984). Les lherzolites associées aux Chaînes Béarnaises (Pyrénées Occidentales): Mise à l'affleurement anté-dogger et resédimentation albo-cénomaniens. *Comptes Rendus de l'Académie des Sciences - Serie II*, 299, 1205-1209.

Elders, Wilfred A., Robert W. Rex, Paul T. Robinson, Shawn Biehler, et Tsvi Meidav. 1972.

831 « Crustal Spreading in Southern California The Imperial Valley and the Gulf of
832 California Formed by the Rifting Apart of a Continental Plate ». *Science* 178 (4056)
833 (juin 10): 15-24. doi:10.1126/science.178.4056.15.

834 Evans, C. A., & Baltuck, M. (1988). Low-Temperature Alteration of Peridotite, Hole 637A.
835 In G. Boillot, E. L. Winterer, & et al. (Éd.), *Proceedings of the Ocean Drilling*
836 *Program, 103 Scientific Results* (Vol. 103, p. 235-239). Ocean Drilling Program.
837 Consulté de http://www-odp.tamu.edu/publications/103_SR/103TOC.HTM

838 Fabriès, J., Lorand, J.-P., & Bodinier, J.-L. (1998). Petrogenetic evolution of orogenic
839 lherzolite massifs in the central and western Pyrenees. *Tectonophysics*, 292(1-2), 145-
840 167. doi:10.1016/S0040-1951(98)00055-9

841 Fabriès, J., Lorand, J.-P., Bodinier, J.-L., & Dupuy, C. (1991). Evolution of the Upper Mantle
842 beneath the Pyrenees: Evidence from Orogenic Spinel Lherzolite Massifs. *Journal of*
843 *Petrology, Special_Volume*(2), 55-76. doi:10.1093/petrology/Special_Volume.2.55

844 Filleaudeau, P.-Y., F Mouthereau, et R. Pik. 2011. « Thermo-tectonic evolution of the south-
845 central Pyrenees from rifting to orogeny: insights from detrital zircon U/Pb and (U-
846 Th)He thermochronometry ». *Basin Research* 23. doi:10.1111/j.1365-
847 2117.2011.00535.x.

848 Folk, R. L. (1974). The natural history of crystalline calcium carbonate: effects of magnesium
849 content and salinity. *J. Sediment. Petrol.*, 44, 40-53.

850 Fortane, A., Duee, G., Lagabrielle, Y., & Coutelle, A. (1986). Lherzolites and the western
851 « Chainons bearnais » (French Pyrenees): Structural and paleogeographical pattern.
852 *Tectonophysics*, 129(1-4), 81-98. doi:10.1016/0040-1951(86)90247-7

853 Früh-Green, G., Weissert, H., & Bernoulli, D. (1990). A multiple fluid history recorded in
854 Alpine ophiolites. *Journal of the Geological Society*, 147(6), 959-970.
855 doi:<p>10.1144/gsjgs.147.6.0959</p>

856 German, C. R., G. P. Klinkhammer, et M. D. Rudnicki. 1996. « The Rainbow Hydrothermal
857 Plume, 36°15'N, MAR ». *Geophysical Research Letters* 23 (21): 2979-2982.
858 doi:10.1029/96GL02883.

859 Gianelli, G., & Principi, G. (1977). Northern Apennine ophiolite: an ancient transcurrent fault
860 zone. *Bolletino della Societa Geologica Italiana*, 96, 53-58.

861 Gibson, I. L., Milliken, K. L., & Morgan, J. K. (1996). Serpentinite-Breccia Landslide
862 Deposits Generated during Crustal Extension at the Iberia Margin. In R. B.
863 Whitmarsh, D. S. Sawyer, A. Klaus, & D. G. Masson (Éd.), *Proceedings of the Ocean*
864 *Drilling Program, 149 Scientific Results* (Vol. 149, p. 571-575). Ocean Drilling
865 Program. Consulté de http://www-odp.tamu.edu/publications/149_SR/149TOC.HTM

866 Golberg, J.-M., & Leyreloup, A. F. (1990). High temperature-low pressure Cretaceous
867 metamorphism related to crustal thinning (Eastern North Pyrenean Zone, France).
868 *Contributions to Mineralogy and Petrology*, 104(2), 194-207.
869 doi:10.1007/BF00306443

870 Golberg, J.-M., & Maluski, H. (1988). Données nouvelles et mise au point sur l'âge du
871 métamorphisme pyrénéen. *C. R. Acad. Sci. Paris*, 306, 429-435.

872 Golberg, J.-M., H. Maluski, et A.-F. Leyreloup. 1986. « Petrological and age relationship
873 between emplacement of magmatic breccia, alkaline magmatism, and static
874 metamorphism in the North Pyrenean Zone ». *Tectonophysics* 129 (1-4) (octobre 15):
875 275-290. doi:10.1016/0040-1951(86)90256-8.

876 Gong, Z., Langereis, C. G., & Mullender, T. A. T. (2008). The rotation of Iberia during the
877 Aptian and the opening of the Bay of Biscay. *Earth and Planetary Science Letters*,
878 273(1-2), 80-93. doi:10.1016/j.epsl.2008.06.016

879 Haggerty, J. A. (1987). Petrology and geochemistry of Neogene sedimentary rocks from
880 Mariana forearc seamounts. In B. H. Keating, P. Fryer, R. Batiza, & G. W. Boehlert
881 (Éd.), *Seamounts, Islands and Atolls* (Am. Geophys. Union, Geophys. Monogr. Ser.,
882 Vol. 43, p. 175-186).

883 Haggerty, J. A. (1991). Evidence from fluid seeps atop serpentine seamounts in the Mariana
884 forearc: Clues for emplacement of the seamounts and their relationship to forearc
885 tectonics. *Marine Geology*, 102(1-4), 293-309. doi:10.1016/0025-3227(91)90013-T

886 Henry, P., Azambre, B., Montigny, R., Rossy, M., & Stevenson, R. K. (1998). Late mantle
887 evolution of the Pyrenean sub-continental lithospheric mantle in the light of new
888 ⁴⁰Ar-³⁹Ar and Sm-Nd ages on pyroxenites and peridotites (Pyrenees, France).
889 *Tectonophysics*, 296(1-2), 103-123. doi:10.1016/S0040-1951(98)00139-5

890 Hervouët, Y., Torné, X., Fortané, A., Duée, G., & Delfaud, J. (1987). Resédimentation
891 chaotique de méta-ophites et de marbres mésozoïques de la vallée du Job (Pyrénées
892 commingeoises): Relations détritisme/métamorphisme en zone nord-Pyrénéenne. *C. R.*
893 *Acad. Sci.*, II, (305), 721-726.

894 Jammes, S., Manatschal, G., Lavier, L. L., & Masini, E. (2009). Tectonosedimentary
895 evolution related to extreme crustal thinning ahead of a propagating ocean: Example
896 of the western Pyrenees. *Tectonics*, 28(4). doi:10.1029/2008TC002406

897 Kelemen, P. B., Kikawa, E., Miller, D. J., & et al. (Éd.). (2004). *Proceedings of the Ocean*
898 *Drilling Program, 209 Initial Reports* (Vol. 209). Ocean Drilling Program. Consulté
899 de http://www-odp.tamu.edu/publications/209_IR/209TOC.HTM

900 Kelley, Deborah S., Jeffrey A. Karson, Donna K. Blackman, Gretchen L. Früh-Green, David

901 A. Butterfield, Marvin D. Lilley, Eric J. Olson, et al. 2001. « An Off-axis
 902 Hydrothermal Vent Field Near the Mid-Atlantic Ridge at 30° N ». *Nature* 412 (6843)
 903 (juillet 12): 145-149. doi:10.1038/35084000.

904 Knipper, A. L. (1978). Ophicalcites and some other types of breccias accompanying the
 905 preorogenic formation of ophiolite complex. *Geotektonika*, 2, 50-66.

906 Knipper, A. L., & Sharas'kin, A. Y. (1998). Exhumation of the upper-mantle and lower-crust
 907 rocks during rifting. *Geotektonika*, 5, 19-31.

908 Lagabriele, Y., & Auzende, J.-M. (1982). Active in situ disaggregation of oceanic crust and
 909 mantle on Gorringe Bank: analogy with ophiolitic massives. *Nature*, 297(5866), 490-
 910 493.

911 Lagabriele, Y., Bideau, D., Cannat, M., Karson, J. A., & Mével, C. (1998). Ultramafic-mafic
 912 plutonic rock suites exposed along the Mid-Atlantic ridge (10°N-30°N). Symmetrical-
 913 asymmetrical distribution and implications for seafloor spreading processes. *Faulting
 914 and magmatism at mid-ocean ridges*, Geophysical monograph (American Geophysical
 915 Union., p. 153-176). Washington, D.C.: Buck W. R., Delaney P. T., Karson J. A.,
 916 Lagabriele Y.

917 Lagabriele, Y., & Bodinier, J.-L. (2008). Submarine reworking of exhumed subcontinental
 918 mantle rocks: field evidence from the Lherz peridotites, French Pyrenees. *Terra Nova*,
 919 20(1), 11-21. doi:10.1111/j.1365-3121.2007.00781.x

920 Lagabriele, Y., & Cannat, M. (1990). Alpine Jurassic ophiolites resemble the modern central
 921 Atlantic basement. *Geology*, 18(4), 319-322. doi:10.1130/0091-
 922 7613(1990)018<0319:AJORTM>2.3.CO;2

923 Lagabriele, Y., Karpoff, A.-M., & Cotten, J. (1992). Mineralogical and Geochemical
 924 Analyses of Sedimentary Serpentinities from Conical Seamount (Hole 788A):
 925 Implication for the Evolution of Serpentine Seamounts. In P. Fryer, J. A. Pearce, L. B.

926 Stokking, & et al. (Éd.), *Proceedings of the Ocean Drilling Program, 125 Scientific*
 927 *Results* (Vol. 125, p. 325-342). Ocean Drilling Program. Consulté de [http://www-](http://www-odp.tamu.edu/publications/125_SR/125TOC.HTM)
 928 [odp.tamu.edu/publications/125_SR/125TOC.HTM](http://www-odp.tamu.edu/publications/125_SR/125TOC.HTM)

929 Lagabriele, Y., Labaume, P., & St Blanquat, M. (2010). Mantle exhumation, crustal
 930 denudation, and gravity tectonics during Cretaceous rifting in the Pyrenean realm (SW
 931 Europe): Insights from the geological setting of the lherzolite bodies. *Tectonics*, 29(4).
 932 doi:10.1029/2009TC002588

933 Lavoie, D., & Cousineau, P. A. (1995). Ordovician ophiolites of southern Quebec
 934 Appalachians; a proposed early seafloor tectonosedimentary and hydrothermal origin.
 935 *Journal of Sedimentary Research*, 65(2a), 337-347. doi:10.1306/D42680B8-2B26-
 936 11D7-8648000102C1865D

937 Laznicka, P. (1988). *Breccias and Coarse Fragmentites: Petrology, Environments,*
 938 *Associations, Ores*. Elsevier Science Ltd.

939 Le Pichon, X., Bonnin, J., & Sibuet, J.-C. (1970). La faille nord-Pyrénéenne: Faille
 940 transformante liée à l'ouverture du Golfe de Gascogne. *Comptes Rendus de*
 941 *l'Académie des Sciences*, D, 271, 1941-1944.

942 Lemoine, M. (1980). Serpentinites, gabbros and ophiolites in the Piemont-Ligurian domain
 943 of the Western Alps: Possible indicators of oceanic fracture zone and of associated
 944 serpentinite protrusions in the Jurassic-Cretaceous Thetys. *Archives des Sciences*
 945 *Genèves*, 33, 103-115.

946 Lemoine, M., Tricart, P., & Boillot, G. (1987). Ultramafic and gabbroic ocean floor of the
 947 Ligurian Tethys (Alps, Corsica, Apennines): In search of a genetic model. *Geology*,
 948 15(7), 622-625. doi:10.1130/0091-7613(1987)15<622:UAGOF>2.0.CO;2

949 Lucazeau, Francis, Sylvie Leroy, Frédérique Rolandone, Elia d' Acremont, Louise Watremez,
 950 Alain Bonneville, Bruno Goutorbe, et Doga Düşünür. 2010. « Heat-flow and

951 hydrothermal circulation at the ocean–continent transition of the eastern gulf of
 952 Aden ». *Earth and Planetary Science Letters* 295 (3–4) (juillet 1): 554- 570.
 953 doi:10.1016/j.epsl.2010.04.039.

954 Manatschal, G. (2004). New models for evolution of magma-poor rifted margins based on a
 955 review of data and concepts from West Iberia and the Alps. *International Journal of*
 956 *Earth Sciences*, 93(3), 432-466. doi:10.1007/s00531-004-0394-7

957 Mattauer, M., & Choukroune, P. (1974). Les Iherzolites des Pyrénées sont des extrusions de
 958 matériel ancien dans le Mésozoïque nord Pyrénées. *paper presented at 2nd Réunion*
 959 *Annuelle des Sciences de la Terre, Soc. Géol. de Fr., Paris*.

960 McCrea, J. M. (1950). On the isotope chemistry of carbonates and a paleotemperature scale.
 961 *J. Chem. Phys.*, 18, 849-857.

962 Milliken, K. L., & Morgan, J. K. (1996). Chemical Evidence for Near-Seafloor Precipitation
 963 of Cacite in Serpentinities (Site 897) and Serpentinite Breccias (Site 899), Iberia
 964 Abyssal Plain. In R. B. Whitmarsh, D. S. Sawyer, A. Klaus, & D. G. Masson (Éd.),
 965 *Proceedings of the Ocean Drilling Program, 149 Scientific Results* (Vol. 149, p. 553-
 966 558). Ocean Drilling Program. Consulté de [http://www-](http://www-odp.tamu.edu/publications/149_SR/149TOC.HTM)
 967 [odp.tamu.edu/publications/149_SR/149TOC.HTM](http://www-odp.tamu.edu/publications/149_SR/149TOC.HTM)

968 Minnigh, L. D., van Calsteren, P. W. C., & den Tex, E. (1980). Quenching: An additional
 969 model for emplacement of the Iherzolite at Lers (French Pyrenees). *Geology*, 8(1), 18.
 970 doi:10.1130/0091-7613(1980)8<18:QAAMFE>2.0.CO;2

971 Moine, B., Fortune, J. P., Moreau, P., & Viguié, F. (1989). Comparative mineralogy,
 972 geochemistry, and conditions of formation of two metasomatic talc and chlorite
 973 deposits; Trimouns (Pyrenees, France) and Rabenwald (Eastern Alps, Austria).
 974 *Economic Geology*, 84(5), 1398 -1416. doi:10.2113/gsecongeo.84.5.1398

975 Monchoux, P. (1970). *Les lherzolites pyrénéennes: contribution à l'étude de leur minéralogie,*
 976 *de leur génèse et de leurs transformations* (Thèse d'Etat). Univ. Toulouse.

977 Montigny, R., Azambre, B., Rossy, M., & Thuizat, R. (1986). K-Ar Study of cretaceous
 978 magmatism and metamorphism in the pyrenees: Age and length of rotation of the
 979 Iberian Peninsula. *Tectonophysics*, 129(1-4), 257-273. doi:10.1016/0040-
 980 1951(86)90255-6

981 Morgan, J. K., & Milliken, K. L. (1996). Petrography of Calcite Veins in Serpentinized
 982 Peridotite Basement Rocks from the Iberia Abyssal Plain, Sites 897 and 899:
 983 Kinematic and Environmental Implications. In R. B. Whitmarsh, D. S. Sawyer, A.
 984 Klaus, & D. G. Masson (Éd.), *Proceedings of the Ocean Drilling Program, 149*
 985 *Scientific Results* (Vol. 149, p. 559-569). Ocean Drilling Program. Consulté de
 986 http://www-odp.tamu.edu/publications/149_SR/149TOC.HTM

987 Muffler, L. J. Patrick, et Donald E. White. 1969. « Active Metamorphism of Upper Cenozoic
 988 Sediments in the Salton Sea Geothermal Field and the Salton Trough, Southeastern
 989 California ». *Geological Society of America Bulletin* 80 (2) (janvier 2): 157-182.
 990 doi:10.1130/0016-7606(1969)80[157:AMOUCS]2.0.CO;2.

991 Muñoz, J. A. (1992). Evolution of a continental collision belt: ECORS-Pyrenees crustal
 992 balanced cross-section. *Thrust Tectonics* (Chapman and Hall., p. 235-246). London:
 993 K. McClay.

994 Ohnenstetter, M. (1979). La série ophiolitifère de Rospigliano (Corse) est-elle un témoin des
 995 phénomènes tectoniques, sédimentaires et magmatiques liés au fonctionnement des
 996 zones transformantes? *Comptes Rendus de l'Académie des Sciences, Paris, D*, 289,
 997 1199-1202.

998 Olivet, J. L. (1996). La cinématique de la plaque ibérique. *Bull. Cent. Rech. Explor. Prod. Elf-*
 999 *Aquitaine*, 20(1), 131-195.

1000 Passchier, C. W. (1984). Mylonite-Dominated Footwall Geometry in a Shear Zone, Central
 1001 Pyrenees. *Geological Magazine*, 121(05), 429-436. doi:10.1017/S0016756800029964
 1002 Peters, T. (1965). A water-bearing andradite from the Totalp serpentine (Davos, Switzerland).
 1003 *Am.*, 50, 1482-1486.
 1004 Picazo, S., Cannat, M., Delacour, A., Escartin, J., Rouméjon, S., & Silantyev, S. (2012).
 1005 Deformation associated with the denudation of mantle-derived rocks at the Mid-
 1006 Atlantic Ridge 13°-15°N: the role of magmatic injections and hydrothermal alteration.
 1007 *Geochemistry Geophysics Geosystems*. doi:10.1029/2012GC004121
 1008 Plas, A. (1997). *Petrologic and stable isotope constraints on fluid-rock interaction,*
 1009 *serpentinization and alteration of oceanic ultramafic rocks* (PhD Thesis). Swiss
 1010 Federal Institute of Technology., Swiss.
 1011 Poujol, M., Boulvais, P., & Kosler, J. (2010). Regional-scale Cretaceous albitization in the
 1012 Pyrenees: evidence from in situ U-Th-Pb dating of monazite, titanite and zircon.
 1013 *Journal of the Geological Society*, 167(4), 751-767. doi:10.1144/0016-76492009-144
 1014 Puigdefàbregas, C., & Souquet, P. (1986). Tecto-sedimentary cycles and depositional
 1015 sequences of the Mesozoic and Tertiary from the Pyrenees. *Tectonophysics*, 129(1-4),
 1016 173-203. doi:10.1016/0040-1951(86)90251-9
 1017 Ravier, J. 1959. « Le métamorphisme des terrains secondaires des Pyrénées ». *Mem. Soc.*
 1018 *Geol. Fr.* 86: 1-250.
 1019 Ross, D. J. (1991). Botryoidal high magnesium calcite cements from the upper Cretaceous of
 1020 the Mediterranean region. *J.*, 61, 349-353.
 1021 Roure, F., & Combes, P.-J. (1998). Contribution of the ECORS seismic data to the Pyrenean
 1022 geology: Crustal architecture and geodynamic evolution of the Pyrenees. Consulté
 1023 de <http://cat.inist.fr/?aModele=afficheN&cpsidt=1874322>

1024 Schärer, U., de Parseval, P., Polvé, M., & St Blanquat, M. (1999). Formation of the Trimouns
1025 talc-chlorite deposit (Pyrenees) from persistent hydrothermal activity between 112 and
1026 97 Ma. *Terra Nova*, 11(1), 30-37. doi:10.1046/j.1365-3121.1999.00224.x

1027 Schwarzenbach, E. (2011). *Serpentinization, fluids and life: comparing carbon and sulfur*
1028 *cycles in modern and ancient environments* (PhD Thesis). Swiss Federal Institute of
1029 Technology., Zurich.

1030 Skelton, A. D. ., & Valley, J. W. (2000). The relative timing of serpentinisation and mantle
1031 exhumation at the ocean-continent transition, Iberia: constraints from oxygen isotopes.
1032 *Earth and Planetary Science Letters*, 178(3-4), 327-338. doi:10.1016/S0012-
1033 821X(00)00087-X

1034 Smart, P. L., Palmer, R. J., Whitaker, F., & Wright, V. P. (1987). Neptunian dikes and
1035 fissures fills: an overview and account of some modern exemples. In N. P. James & P.
1036 W. Choquette (Éd.), *Paleokarst* (Springer-Verlag., p. 149-163). New York.

1037 Souquet, P., Debroas, E.-J., Boirie, J.-M., Pons, P., Fixari, G., Dol, J., Thieuloy, J.-P., et al.
1038 (1985). Le groupe du Flysch noir (albo-cénomaniens) dans les Pyrénées. *Bull. centres*
1039 *de Rech. Explor.-Prod. Elf-Aquitaine, Pau*, 9(1), 183-252.

1040 Spooner, E. T. C., & Fyfe, W. S. (1973). Sub-sea-floor metamorphism, heat and mass
1041 transfer. *Contributions to Mineralogy and Petrology*, 42(4), 287-304.
1042 doi:10.1007/BF00372607

1043 St Blanquat, M. (1993). La faille normale ductile du massif du Saint Barthélémy: Evolution
1044 hercynienne des massifs nord-pyrénéens catazonaux considérée du point de vue de
1045 leur histoire thermique. *Geodin. Acta*, 6(1), 59-77.

1046 St Blanquat, M., Brunel, M., & Mattauer, M. (1986). Les zones de cisaillements du massif
1047 nord Pyrénéen du Saint-Barthelemy, témoins probables del'extension crustale d'âge
1048 crétaé. *C*, 303, 1339-1344.

1049 St Blanquat, M., Lardeaux, J. M., & Brunel, M. (1990). Petrological arguments for high-
 1050 temperature extensional deformation in the Pyrenean Variscan crust (Saint Barthélémy
 1051 Massif, Ariège, France). *Tectonophysics*, 177(1-3), 245-262. doi:10.1016/0040-
 1052 1951(90)90284-F

1053 Surour, A. A., & Arafa, E. H. (1997). Ophicarbonates: calichified serpentinites from Gebel
 1054 Mohagara, Wadi Ghadir area, Eastern Desert, Egypt. *Journal of African Earth*
 1055 *Sciences*, 24(3), 315-324. doi:10.1016/S0899-5362(97)00046-8

1056 Teixell, A. (1998). Crustal structure and orogenic material budget in the west central
 1057 Pyrenees. *Tectonics*, 17(3), 395-406. doi:199810.1029/98TC00561

1058 Ternet, Yves, M. Colchen, Elie-Jean Debroas, B. Azambre, F. Debon, J.-L. Bouchez, G.
 1059 Gleizes, et al. 1997. *Notice explicative, Carte géol. France (1/50 000), feuille Aulus*
 1060 *les Bains (1086)*. BRGM éd. Orléans: BRGM.

1061 Thiébaud, J., Debeaux, M., Durand-Wackenheim, C., Souquet, P., Gourinard, Y., Bandet, Y.,
 1062 & Fondecave-Wallez, M.-J. (1988). Métamorphisme et halocinèse crétacés dans les
 1063 évaporites de Betchat le long du chevauchement frontal Nord-Pyrénéen (Haute-
 1064 Garonne et Ariège, France). *C. R. Acad. Sci. Paris*, 307(13), 1535-1540.

1065 Thiébaud, J., Durand-Wackenheim, C., Debeaux, M., & Souquet, P. (1992). Métamorphisme
 1066 des évaporites triasiques du versant nord des Pyrénées centrales et Occidentales. *Bull.*
 1067 *Soc. Hist. Nat. Toulouse*, 128, 77-84.

1068 Treves, B. E., & Harper, G. D. (1994). Exposure of serpentinites on ocean floor. Sequence of
 1069 faulting and hydrofracturing in the Northern Apennine ophicalcites. *Ophioliti*, 19, 435-
 1070 466.

1071 Treves, B. E., Hickmott, D., & Vaggelli, G. (1995). Texture and microchemical data of
 1072 oceanic hydrothermal calcite veins, Northern Apennine ophicalcites. *Ophioliti*, 20(2),
 1073 111-122.

- 1074 Trommsdorff, V., Evan, B. W., & Pfeifer, H. R. (1980). Ophicarbonates: metamorphic
1075 reactions and possible origin. *Archives des Sciences Genève*, 33, 361-364.
- 1076 Valley, J.W., 1986. Stable isotope geochemistry of metamorphic rocks. In: Valley, J.W.,
1077 Taylor, H.P., Jr., O'Neil, J.R. Eds., Stable Isotopes in High Temperature Geological
1078 Processes. *Reviews in Mineralogy*, Vol. 16. Mineral. Soc. Am., 445-489.
- 1079 Vergés, J., & Garcia-Senz, J. (2001). Mesozoic evolution and Cainozoic inversion of the
1080 Pyrenean rift. *Peri-Tethys Memoir 6: Peri-Tethyan Rift/Wrench Basins and Passive*
1081 *Margins* (Mem. Mus. Natl. Hist. Nat., p. 187-212). Paris: P. A. Ziegler et al. Consulté
1082 de http://www.ija.csic.es/gt/gdl/jverges/PDF/Verges_Garcia_2001.pdf
- 1083 Vielzeuf, D. (1984). *Relations de phases dans le faciès granulite et implications*
1084 *géodynamiques. L'exemple des granulites des pyrénées*. (Thèse). Clermont-Ferrand.
- 1085 Vielzeuf, D., & Kornprobst, J. (1984). Crustal splitting and the emplacement of Pyrenean
1086 lherzolites and granulites. *Earth and Planetary Science Letters*, 67(1), 87-96.
1087 doi:10.1016/0012-821X(84)90041-4
- 1088 Vissers, R. L. M., Drury M. R., Newman J., & Fliervoet T. F. (1997). « Mylonitic
1089 deformation in upper mantle peridotites of the North Pyrenean Zone (France):
1090 implications for strength and strain localization in the lithosphere ». *Tectonophysics*,
1091 279, 303-325. doi:10.1016/S0040-1951(97)00128-5.
- 1092 Weissert, H., & Bernoulli, D. (1984). Oxygen isotope composition of calcite in Alpine
1093 ophicarbonates: a hydrothermal or Alpine metamorphic signal? *Eclogae geol. Helv.*,
1094 77(1), 29-43.
- 1095 Wicks, F. J., & Whittaker, E. J. W. (1977). Serpentine textures and serpentinization. *The*
1096 *Canadian Mineralogist*, 15(4), 459 -488.

1097 Winterer, E. L., Metzler, C. V., & Sart, M. (1991). Neptunian dykes and associated breccias
1098 (Southern Alps, Italy and Switzerland): role of gravity sliding in open and closed
1099 systems. *Sedimentology*, 38(3), 381-404. doi:10.1111/j.1365-3091.1991.tb00358.x
1100 Zheng, Y. F. (2011). On the theoretical calculations of oxygen isotope fractionation factors
1101 for carbonate-water systems. *Geochemical Journal*, 45, 341-354.
1102

1103 **Table Caption**

1104

1105 **Table 1:** C (vs. PDB) an O (vs. SMOW) isotopes compositions determined for the carbonate

1106 fraction of the veins, matrix and clasts from the Pyrenean ophicalcite.

1107 **Table 2:** Schematic representation of the different types of ophicalcites analyzed in this study.

1108

Figure Caption

Figure 1. Simplified geological map of the Northern Pyrenean belt with location of the peridotite bodies sampled in this study.

Figure 2. A: Simplified geological map of the Urdach and Tos de la Coustette in the Mail Arrouy and Sarrance *Chaînon Béarnais* with sample sites. B: Simplified geologic map of the Aulus basin presenting the extent of exposure of the peridotite bearing deposits surrounding the *Etang de Lherz* area with the location of the Freychinède, Fontête Rouge, and Berqué samples sites.

Figure 3: Photograph of an ultramafic olistolith in the Aulus basin illustrating the progressive transition from polymictic breccias to massive peridotite penetrated by calcitic veins

Figure 4: Macroscopic aspects of some of the western Pyrenean ophicalcites. A and B: development of calcites veins along tectonic discontinuities in the Urdach peridotite body. C: Mesh texture in highly serpentinized peridotite of Tos de la Coustette. D: Pervasive carbonation and veins in Tos de la Coustette peridotite. Calcite veins (E) and cavities infillings (F) in the Moncaup ultramafic body.

Figure 5: Macroscopic aspects of some of the eastern Pyrenean ophicalcites. A: Bimodal litharenite presenting slumps and syn-sedimentary normal faults from Lherz. B: Grain sorting

1131 in polymictic litharenites from Lherz. C and D: Breccia reworking fresh (orange to green) and
1132 serpentinized (dark green to black) peridotites in a calcitic matrix from the Lherz ophicalcites.
1133 E: Close association of matrix and veins in a typical ophicalcite from Vicdessos. F: Exposure
1134 of an ultramafic body presenting a centimetric orange-brown oxidation ring on the contact
1135 between peridotites and carbonates (Ercé-Angladure) G: Metric-sized mesh texture in the
1136 Bestiac peridotites. H: Detail of F showing calcite veins cross-cutting the latest serpentinite
1137 veins.

1138

1139 Figure 6: Microscopic aspects of the Pyrenean ophicalcites. A: Seal crack calcite vein from
1140 Urdach in cathodoluminescence (CL) and redrawn. B: Micrometric veinlets from Urdach. C:
1141 Botryoidal calcite in a vein from Urdach, in transmitted light and CL. D: Replacement texture
1142 of the ophicalcites from Tos de la Coustette, polarized light. F: Clear sparry calcite in veins
1143 from Lherz. G: Close vein/matrix association in transmitted light and CL. H: Dogtooth calcite
1144 ghosts in recrystallized veins, in polarized light and Redrawn.

1145

1146 Figure 7: $\delta^{13}\text{C}$ vs. $\text{d}18\text{O}$ diagram showing the isotopic compositions of the Pyrenean
1147 ophicalcites (veins, matrices and clasts). Shaded areas represent values from the literature for
1148 ophicalcites from the Iberian margin and Galicia bank (Evans & Baltuck 1988; Milliken &
1149 Morgan 1996; Plas 1997; Skelton & Valley 2000); the Alps and Apennines (Brotzu et al.
1150 1973; Barbieri et al. 1979; Weissert & Bernoulli 1984; Barrett & Friedrichsen 1989; Demeny
1151 et al. 2007) and from other hydrothermal ophicalcites (Lavoie & Cousineau 1995; Artemyev
1152 & Zaykov 2010).

1153

1154 Figure 8: Comparison of the C and O isotope compositions of calcitic veins and matrices in
1155 the ophicalcites from Eastern Pyrenees.

1156

1157 Figure 9: Comparison of calcite microtextures in veins and matrices from this study and from
1158 the Iberian margin (Morgan & Milliken, 1996).

1159

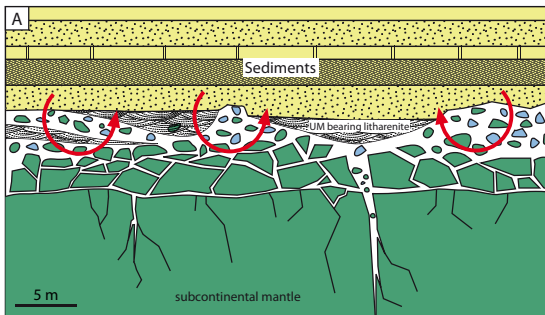
1160 Figure 10: Cartoons illustrating the three possible mechanisms responsible the low O
1161 composition of the sedimentary ophicalcites from the Eastern Pyrenees.

1162

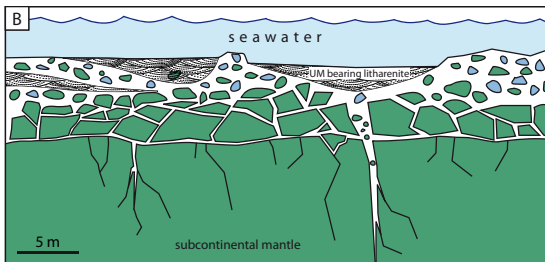
1163 Figure 11: Sketches presenting the exhumation history of the Eastern and Western Pyrenean
1164 peridotites in the light of our isotope study. Serpentinization processes are represented by
1165 green colors and the formation of ophicalcites by blue colors.

1166

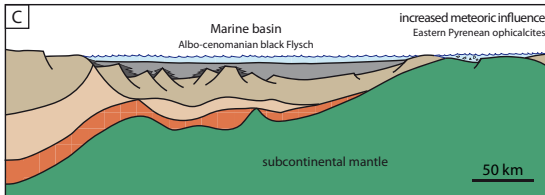
Post-metamorphic
metamorphic imprint



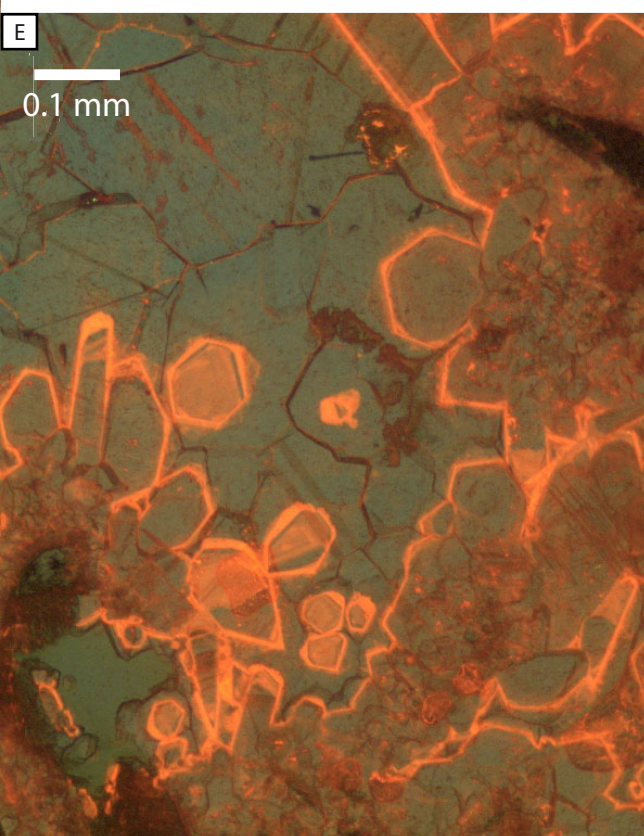
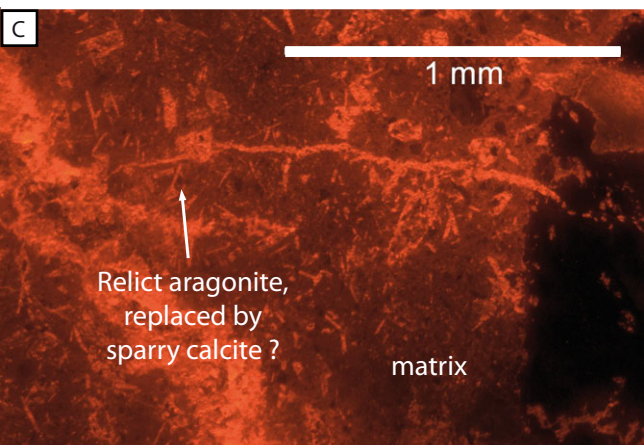
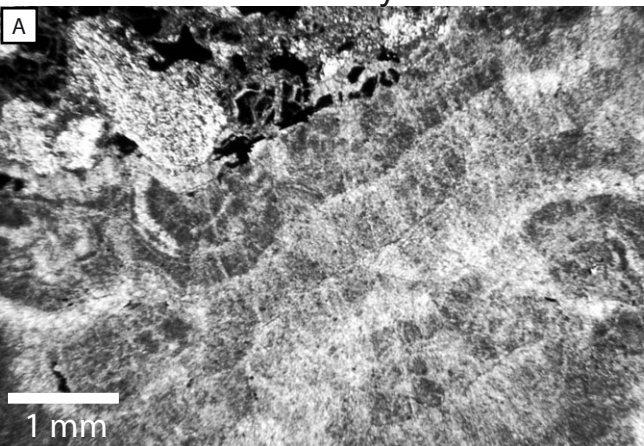
Precipitation from
hot pore-water



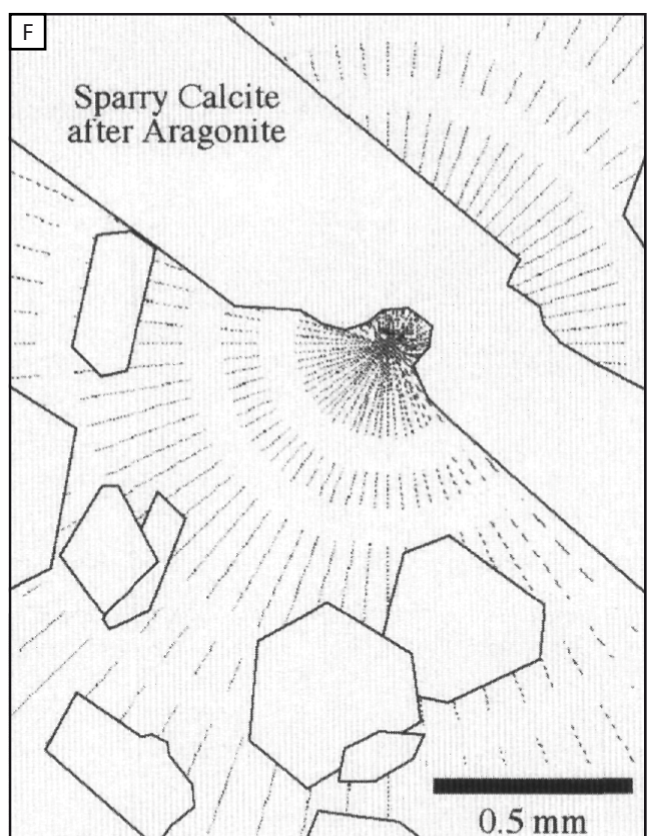
Precipitation from
continental waters

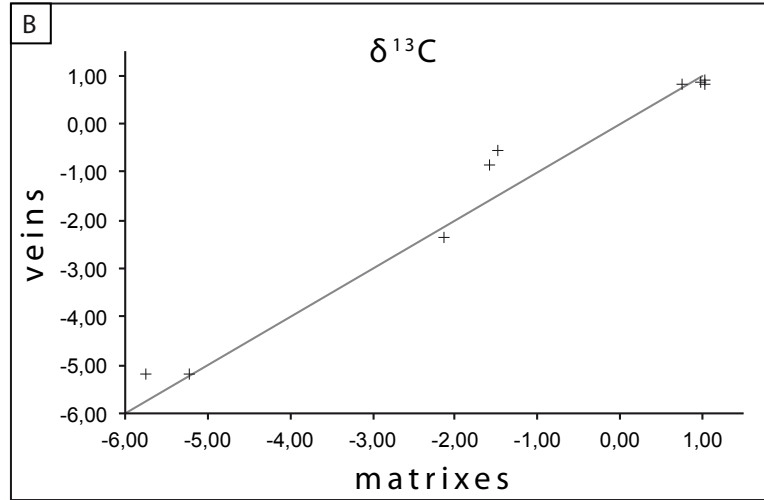
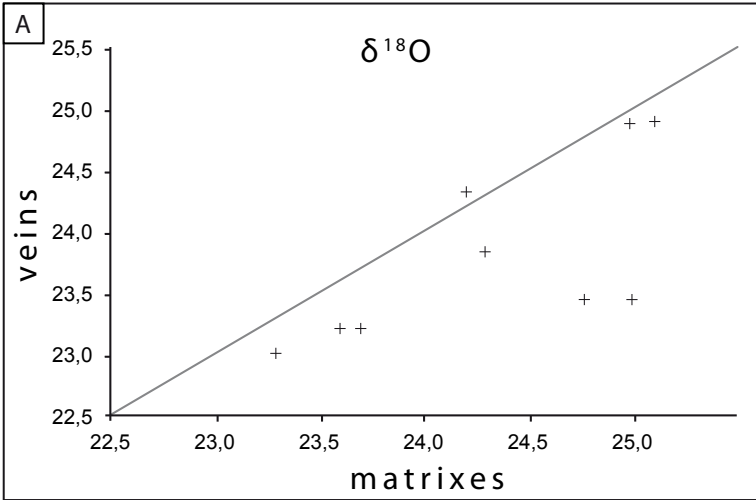


This study

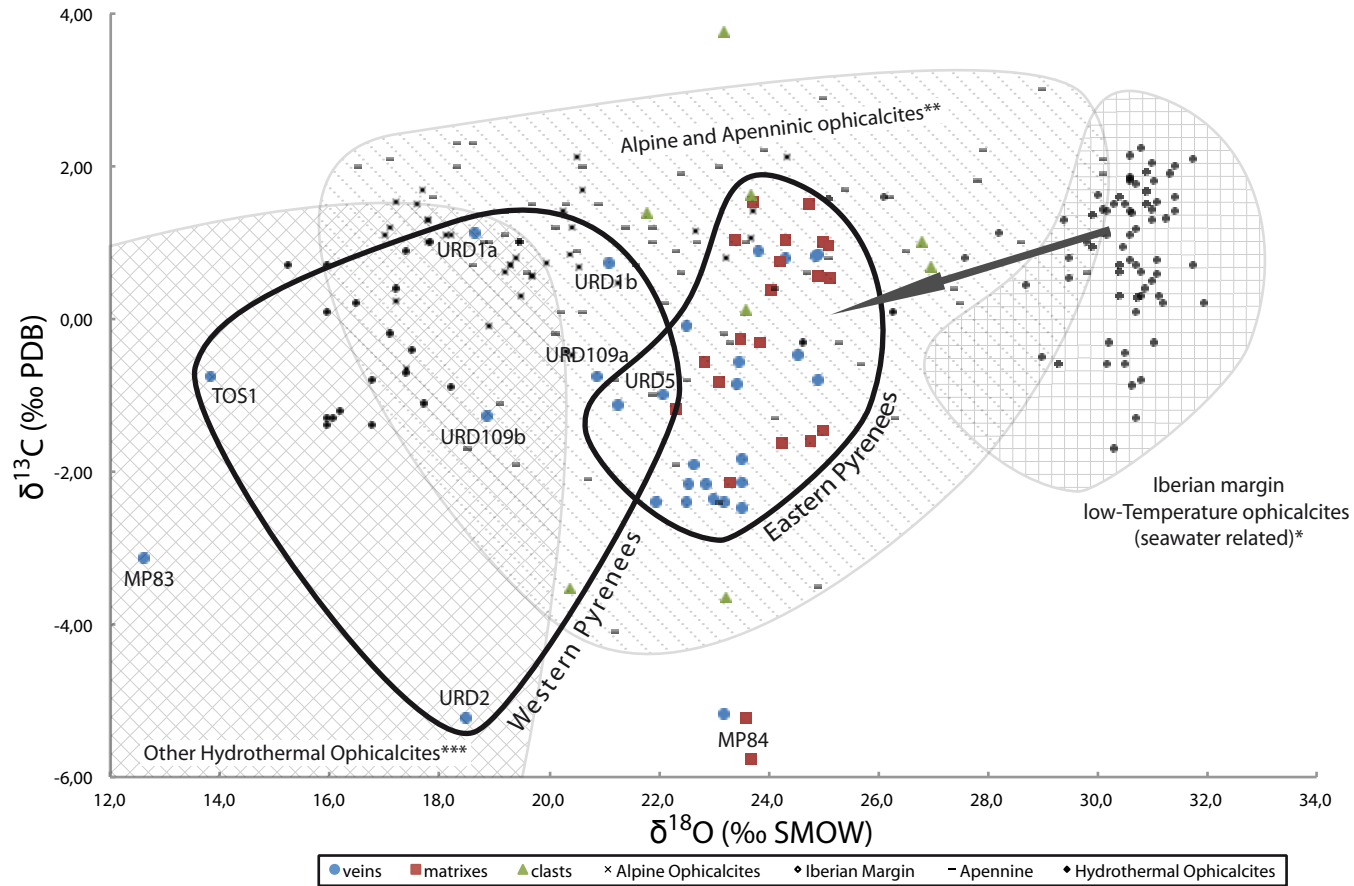


Morgan & Milliken (1996)

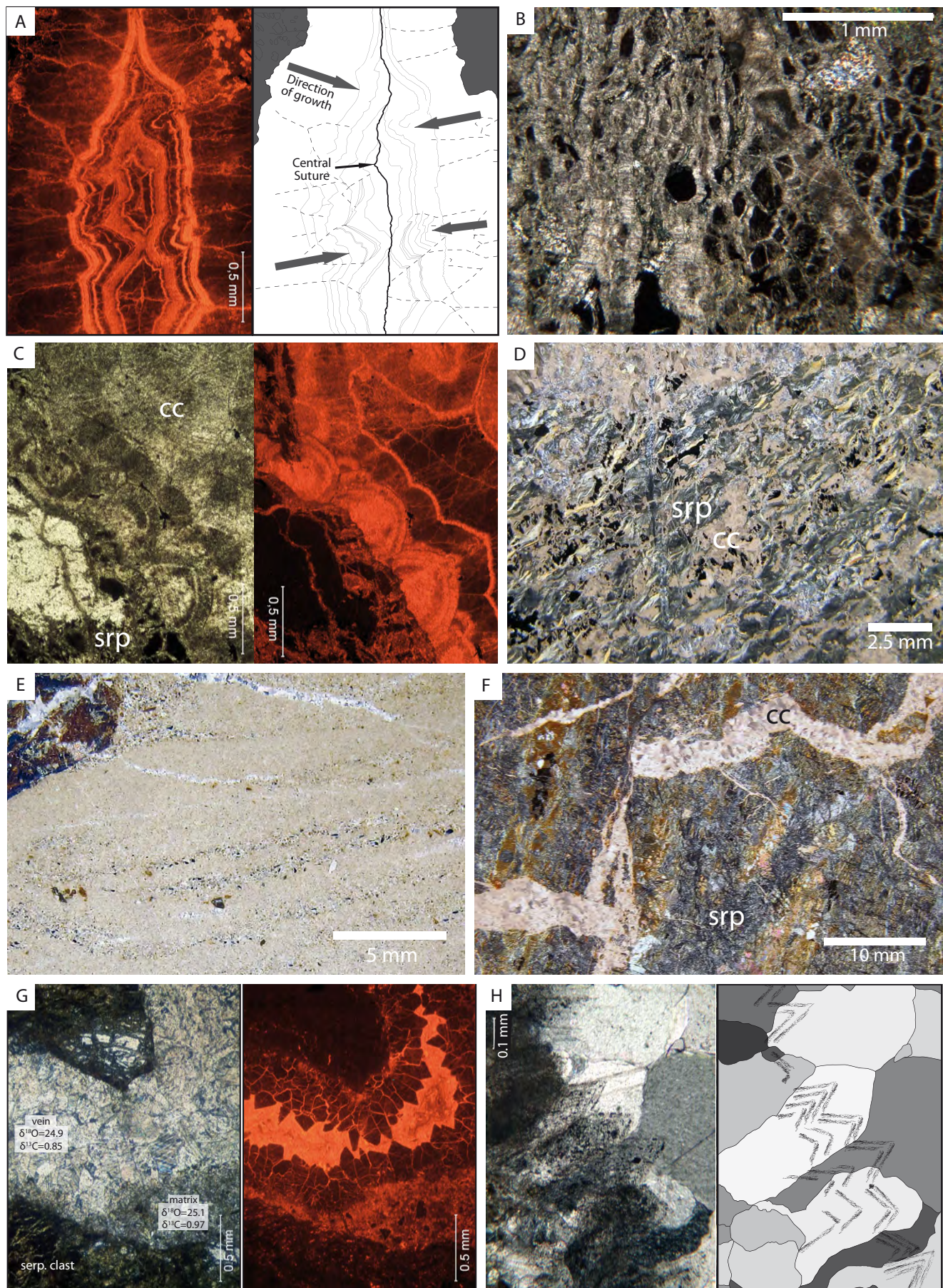


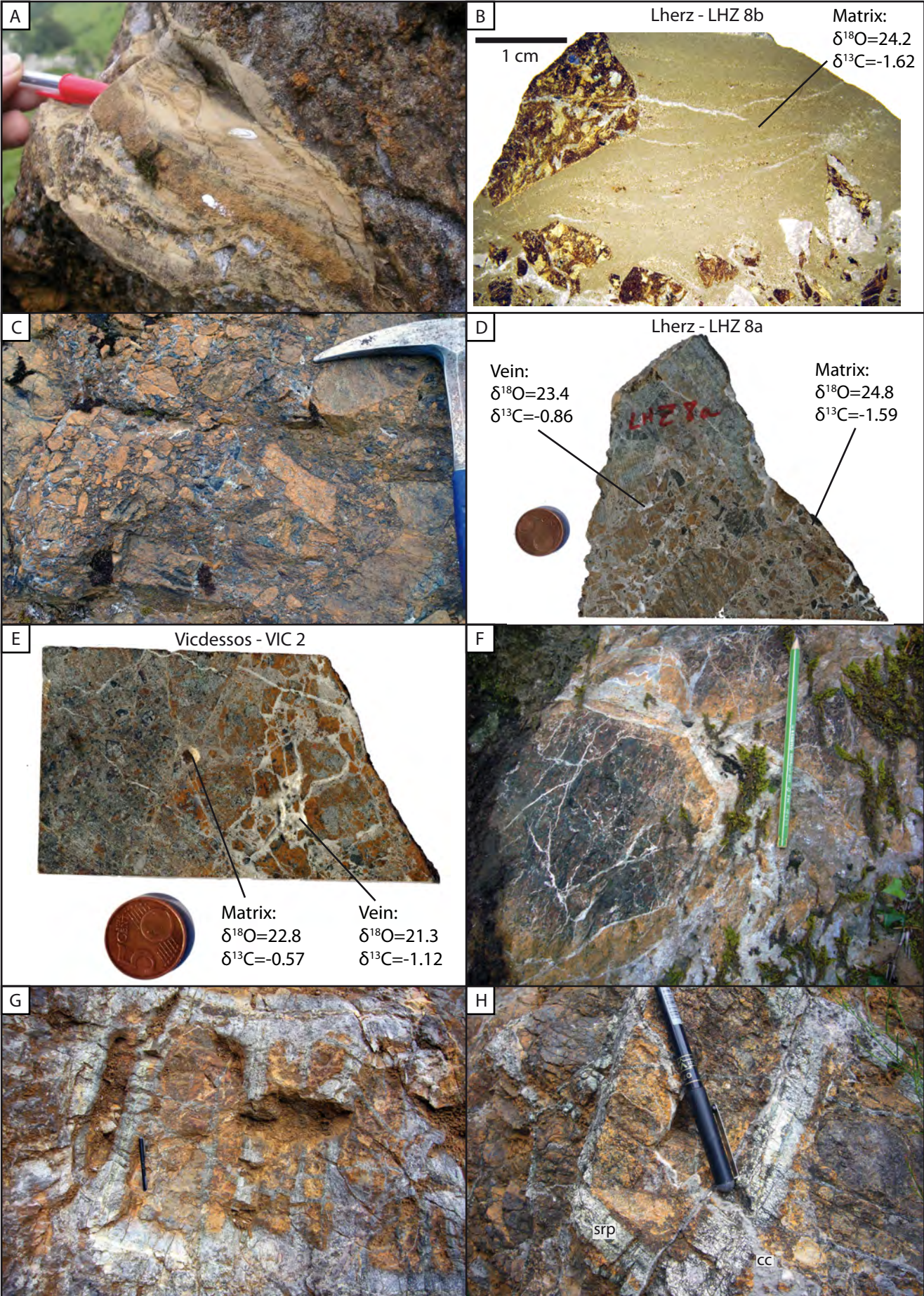


Clerc et al - IJES - Submitted - Figure 8



Clerc et al - IJES - Submitted - Figure 7





A



B

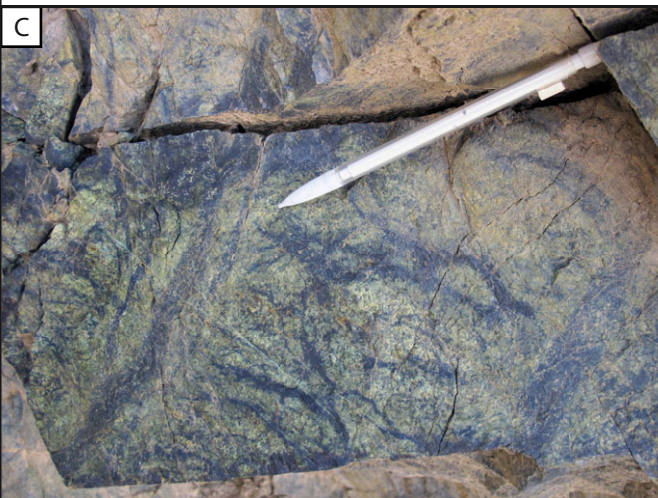
Urdach - URD 1

Vein:
 $\delta^{18}\text{O}=21.1$
 $\delta^{13}\text{C}=0.73$



Vein:
 $\delta^{18}\text{O}=18.6$
 $\delta^{13}\text{C}=1.12$

C



D

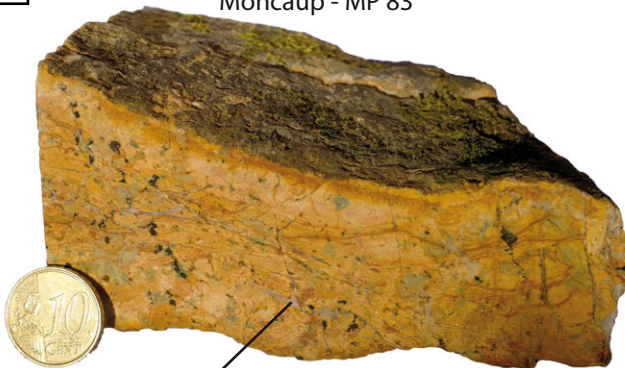
Tos de la Coustette - TOS 1

Vein:
 $\delta^{18}\text{O}=13.8$
 $\delta^{13}\text{C}=-0.76$



E

Moncaup - MP 83



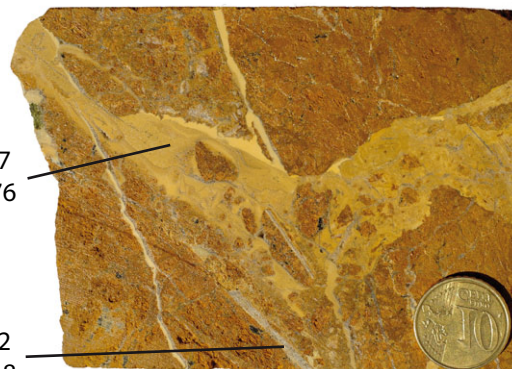
Vein:
 $\delta^{18}\text{O}=12.6$
 $\delta^{13}\text{C}=-3.12$

F

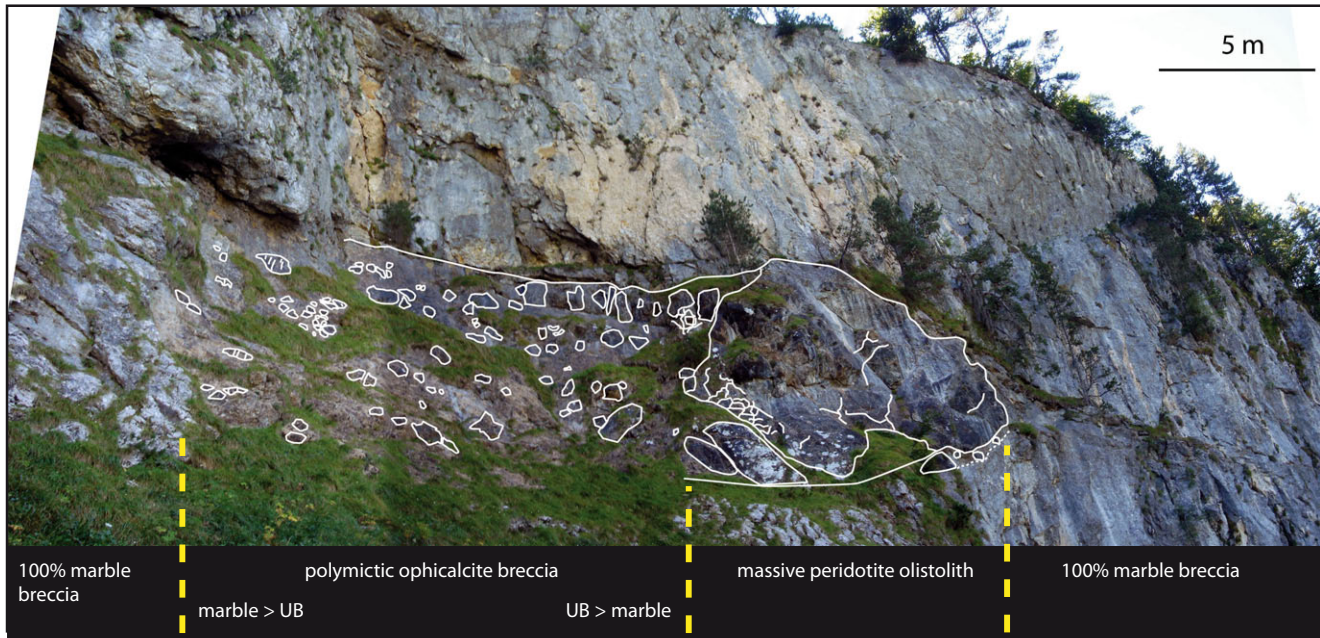
Moncaup - MP 84

Matrix:
 $\delta^{18}\text{O}=23.7$
 $\delta^{13}\text{C}=-5.76$

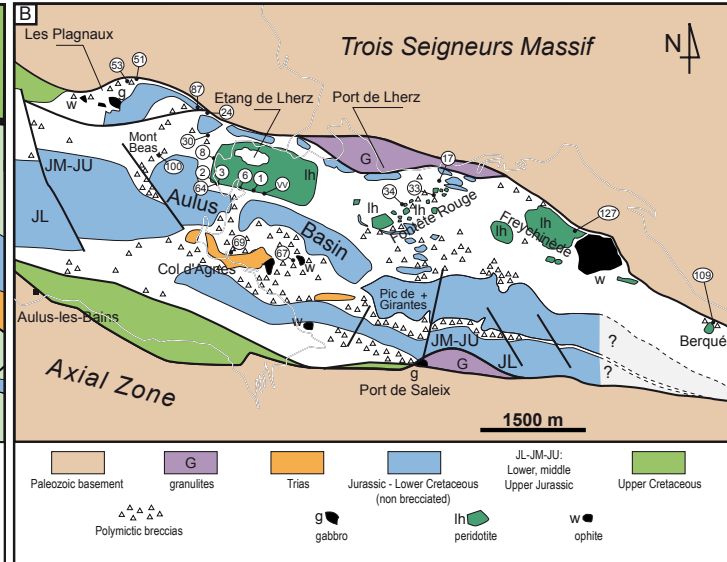
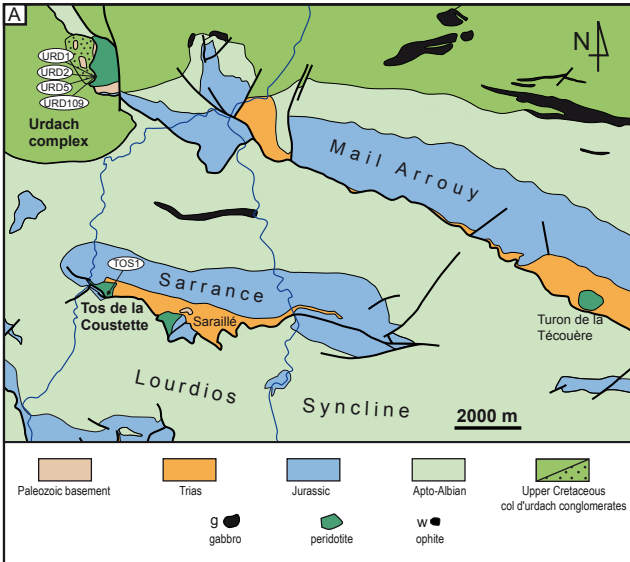
Vein:
 $\delta^{18}\text{O}=23.2$
 $\delta^{13}\text{C}=-5.18$



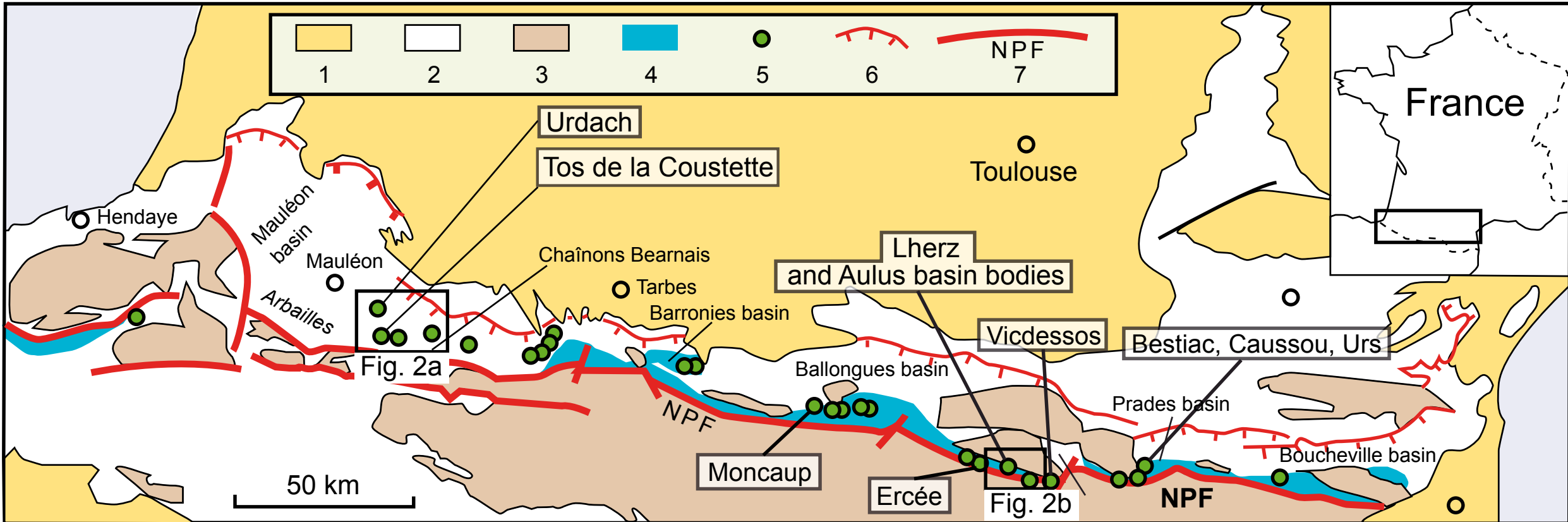
5 m



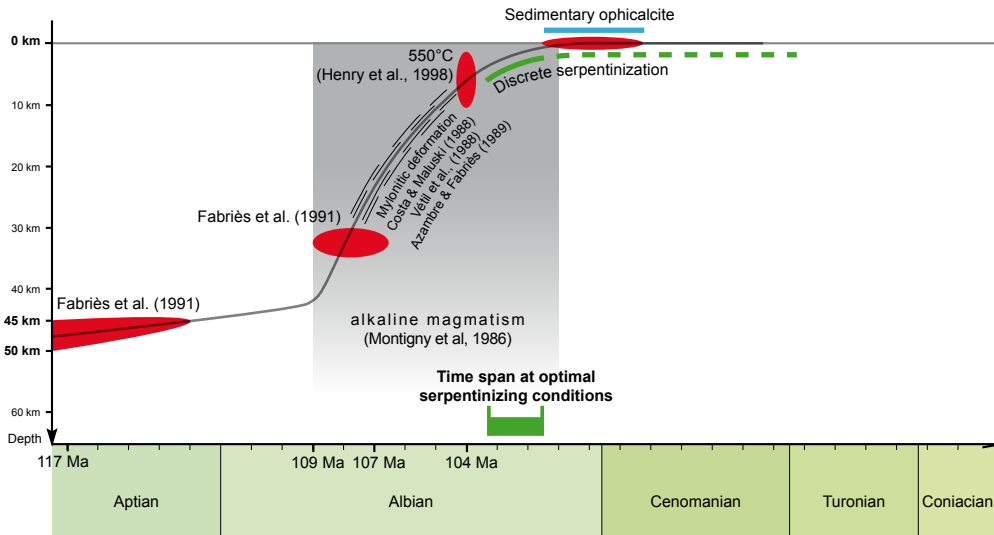
Clerc et al - IJES - Submitted - Figure 3



Clerc et al - IJES - Submitted - Figure 2



EASTERN Peridotite



WESTERN Peridotite

